RSC Medicinal Chemistry

ROYAL SOCIETY OF CHEMISTRY

REVIEW

View Article Online
View Journal | View Issue

Check for updates

Cite this: *RSC Med. Chem.*, 2025, **16**, 4657

Naphthalimide–organometallic hybrids as multi-targeted anticancer and luminescent cellular imaging agents

David C. Magri * and Alex D. Johnson

Received 7th March 2025,
Accepted 17th July 2025

DOI: 10.1039/d5md00205b

rsc.li/medchem

1,8-Naphthalimides with an organometallic moiety with anticancer and luminescence or photoactive properties are reviewed. Primarily highlighted are 1,8-naphthalimide complexes with iron, platinum, and ruthenium, while honourable mentions are given to iridium, rhenium and rhodium complexes. The cytotoxicity, mechanism of action and cell selectivity of the compounds are discussed alongside their photophysical properties for monitoring interactions with biomolecules, most notably DNA, by absorption, fluorescence and dichroism spectroscopy. The luminescence properties provide additional insight regarding the cellular uptake and location of the intelligent agents within both cancer and healthy cells. The versatility of this emerging hybrid class of molecules earmarks them as multi-functional therapeutic and cellular imaging agents. The review concludes with suggestions for designing more effective multi-targeting cytotoxic agents with improved biocompatibility and imaging in hopes of enhancing their clinical potential.

Introduction

Cancer is a generic term for more than a hundred types of related diseases.[1] A defining feature of the disease is the rapid growth of abnormal cells beyond their traditional boundary, and in later stages, the spreading of the abnormal cells to other organs, or parts of the body (referred to as metastasis). The World Health Organization (WHO) reported that cancer is the second leading cause of mortality worldwide accounting for nearly 10 million deaths in 2020.[2] By 2030, the International Agency for Research on Cancer (WHO cancer research agency) estimates that the number of cases will increase to 13 million deaths. Cancer chemotherapy[3] has been prevalent in society for decades with much success; however, the methods for treating this broadly defined disease are not without debilitating side effects. Many challenges remain such as cancer cell resistance to medicines including the expulsion of many drugs by P-glycoproteins, selectivity of the drug for cancer cells, and avoidance of the healthy unaffected cells.[4] The conventional target-based approach to cancer drug discovery has provided many drug entities, notably platinum (Pt)-based drugs. However, it is widely acknowledged that for such a complex disease, a more diverse strategy with multiple modes of action is needed rather than the traditional selection of a single, specific target.[5–7]

Department of Chemistry, Faculty of Science, University of Malta, Msida, MSD 2080, Malta. E-mail: david.magri@um.edu.mt; Tel: +(356) 2340 2276

Three Pt-based complexes are approved worldwide for cancer treatment: cisplatin, carboplatin, and oxaliplatin (Fig. 1). Cisplatin **1**, the first Pt metallodrug,[8] is an antineoplastic that covalently binds to deoxyribonucleic acid (DNA) by forming Pt–DNA adducts at the N7 positions of guanine (G) and adenosine (A) bases to afford 1,2 and 1,3-intrastrand crosslinks.[3,4] This event inhibits cell replication and transcription, while eventually promoting cell death by apoptosis. Cisplatin also forms adducts in mitochondrial DNA (mtDNA) lacking histones.[3] It interacts with thiol-containing peptides, proteins, and RNA and binds to phospholipids and phosphatidylserine of the cell membrane. These unintended interactions are a source of resistance development and toxicity. An important non-DNA target of cisplatin is the tripeptide glutathione (GSH), which is present in cells at 1.0–10 mM. For binding to genomic or mitochondrial DNA, cisplatin must lose at least one of its chloride atoms. Hydrolysis of one or both chloride atoms results in the formation of aquo species, eventually the

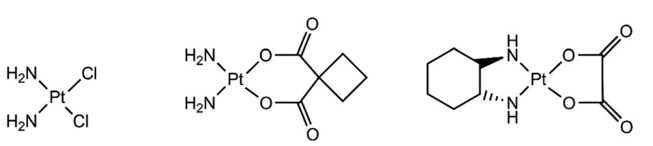

Fig. 1 The three most widely used platinum drugs for treating cancer.

$[Pt(H_2O)_2(NH_3)_2]^{2+}$ cation. Water is a better leaving group than chloride, so the aquo species are more reactive towards nucleophilic biomolecules containing thiols.

Carboplatin **2** is an analogue of cisplatin with the two chlorides replaced by a chelated dicarboxylate ligand (1,2-cyclobutanedicarboxylate), which decreases toxicity and confers improved chemical stability and good aqueous solubility.[9] As the chloride concentration within cells ranges from 2–30 mM, hydrolysis of carboplatin to the diaqua Pt complex is more facile than cisplatin. Oxaliplatin **3**, a treatment for colorectal and advanced ovarian cancers, is covalently derivatised with a bidentate *trans*-1,2-diaminocyclohexane and an oxalate ligand.[10] The oxalate moiety is displaced to give mono and diaqua species that react with the DNA bases. Other structural Pt analogues have come available in Asia.[11]

Despite these many successes, one-third of cancers remain non-responsive to Pt drugs. A quest remains for cancer chemotherapeutics that combine (1) high efficiency, (2) low patient toxicity, and (3) different and multiple mechanisms of action while dealing with the practical issues of biocompatibility including water solubility, undesired side effects and cancer cells developing resistance. Resistance to cancer medications can occur by various mechanisms comprising (1) reduced uptake of the drug and/or increased efflux, (2) increased cellular thiol levels, (3) enhanced DNA repair and/or increased damage tolerance, and (4) failure of cell-death apoptosis pathways. It is envisioned that new drugs with multiple modes of action will overcome resistance development by cancer cells.

1,8-Naphthalimides (benz[de]isoquinolin-1,3-diones) are a remarkable class of dyes and known antineoplastic agents against various human cancer cell lines.[12–18] They are relatively immune to efflux by glycoproteins. Many candidates have progressed to clinical trials, but most do not advance beyond the later stages of clinical trials due to severe side effects. A common mechanistic target is non-covalent binding or intercalation to DNA within the nucleus of the cancer cell. The planar structure of the π-aromatic core (Fig. 2) facilitates insertion between DNA base pairs, although interactions are also possible with the double helix minor and major grooves. Substituents with positively charged amines at the imide and/or 3- and 4-positions further strengthen intermolecular interactions with the negatively charged DNA phosphate backbone. When bound to DNA, the naphthalimide–DNA complex inhibits the functioning of topoisomerase I and II enzymes, and may trigger apoptosis.[19]

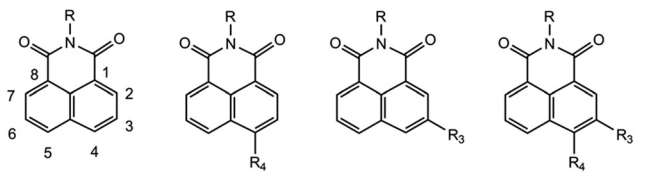

Fig. 2 The naphthalimide core structure with position numbering 1–8 and the three most common substitution patterns.

In addition, naphthalimides are known to invoke cytotoxicity *via* mitochondria-induced lysosomal membrane permeabilization.[20] Naphthalimides with multiple modes of action could thwart cancer cells from developing resistance, which is a reason why they continue to be explored as potential cancer drugs.

Functionalisation of 1,8-naphthalimides with a heteroatom, typically nitrogen or oxygen, at the 2, 3 or 4-position of the naphthalene ring provides compounds with internal charge transfer (ICT) transitions.[21–23] These modifications introduce enhanced electronic and optical properties and solvatochromic effects with a strong emission, typically a green colour at about 500 nm, although other colours of the rainbow associated with longer emission wavelengths can be obtained by careful alteration of the ring substituents. Hence, the DNA binding modes with 1,8-naphthalimides can be assessed by UV-vis absorption, fluorescence and circular dichroism spectroscopy techniques.[24] The tunable optical properties of 1,8-naphthalimides combined with their antineoplastic nature allow them to be exploited as intelligent agents with therapeutic and imaging diagnostic uses.[25]

Classification of compounds based on cytotoxicity and luminescence

To be successful in the fight against cancer, a portfolio of chemical entity classifications is proposed with varying cytotoxicity and luminescence properties for understanding the mechanism of action as well as treatment.[26] Fig. 3 is a matrix classifying compounds into one of four categories based on the cytotoxicity and/or luminescence properties. The four categories are (1) reference compounds, (2) optical probes, (3) traditional medicines and (4) theranostics. A compound is defined as having good cytotoxicity when the $IC_{50} < 10$ μM and having weak cytotoxicity when the $IC_{50} > 50$ μM, and moderate cytotoxicity within this range. Similarly, a compound is defined as being highly luminescent when the (fluorescence) quantum yield $\Phi_f > 0.10$, and non-

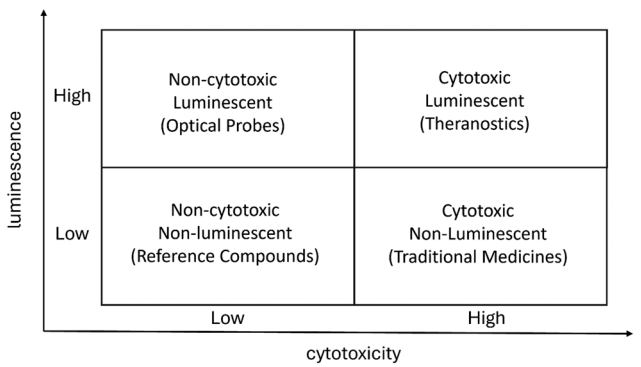

Fig. 3 A matrix categorising compounds into four groups based on the cytotoxicity and luminescence properties. High cytotoxicity is defined when the $IC_{50} < 10$ μM and high luminescence when the $\Phi_f > 0.010$.

luminescent when $\Phi_f < 0.02$, which is near the naked-eye limit of detection. The high and low ratio for both IC_{50} and Φ_f is set at a factor of 5. The middle range in between for both the cytotoxicity and luminescence allows for some flexibility in setting the threshold level.

The first category of compounds is those with low cytotoxicity ($IC_{50} > 50$ μM) and that are non-luminescent ($\Phi_f < 0.02$). Such compounds lacking the desired properties might be considered irrelevant and quickly passed over during screening for they would be considered negative results towards the treatment of cancer (Fig. 3, bottom left quadrant). However, such chemical entities are the reference compounds (what not to do) for designing a better therapeutic drug.

The second category of compounds is those with cytotoxicity <10 μM, which are considered potential lead candidates within the definition of medicinal chemistry, and lacking any luminescence properties ($\Phi_f < 0.02$) (Fig. 3 bottom, right quadrant). The early history of Pt organometallic drugs that covalently bind and/or intercalate with DNA fits this category.[27]

The third category of compounds is those with low cytotoxicity ($IC_{50} > 50$ μM) and with luminescence properties ($\Phi_f > 0.02$) for *in vivo* and *in vitro* imaging. They can be used to track their location within a cell or living organism.[28] This is the field of fluorescent tags, such as ethidium bromide, and optical probes and chemosensors (Fig. 3, top left quadrant). A high luminescence response may result from intercalation with DNA,[29] capture or displacement of an analyte, or in response to a microenvironmental condition (*i.e.* polarity). A luminescent indicator can be used to advantageously confirm entrance into a cell. Once in the cell, a secondary function of the probe is to report on its location within the cell. With modern technology, the journey of molecules can be tracked using real-time imaging such as confocal fluorescence and super-resolution microscopy.

The fourth and final category of compounds combines the properties of high luminescence ($\Phi_f > 0.10$) with high cytotoxicity (<10 μM). The diagnosis and treatment of disease by combining targeted drugs and luminescence imaging, among other types, is the field of theranostics (Fig. 3, top right quadrant).[30] A cytotoxic medicine with a luminescence response can communicate its presence within a cell and provide mechanistic information in real time. Examples of dual-mode drugs with luminescent reporting units are acridine orange and 9-aminoacridine.[31,32]

Trackable therapeutic agents[33] are becoming increasingly intelligent. They can communicate valuable information on acidity, analyte concentrations and the overexpression of proteins. Dual-functional molecules with luminescence properties can provide insight into the mechanism of action enabling a deeper understanding of the biological behaviour. Naturally this is easiest with 4-amino-1,8-naphthalimides with their illuminating green emission at the cellular level. Clinical applications require molecules that emit at longer wavelengths for light to penetrate tissue during photodynamic therapy (PDT)[34] at a wavelength of irradiation of typically 600–900 nm. A further level of sophistication involves the rational design of compounds that are non-cytotoxic ($IC_{50} > 50$ μM) upon first entry into the cell (dark state), which upon exposure to light become cytotoxic ($IC_{50} < 10$ μM) at a localised site, and in many instances, luminescent too. Compounds with these characteristics are referred to as photocytotoxic. In the following sections, naphthalimide–organometallic compounds possessing cytotoxicity toward cancer cells with luminescence properties are presented.

Molecular engineering of multi-purpose molecules

Our initial objective was to design intelligent molecules as fluorescent lab-on-a-molecule systems for detecting multiple clinical parameters.[35,36] We were not considering specific drug targets. Our strength was engineering molecules that sense cations and anions, and protons (pH) and oxidising (pE) conditions by modulation of a fluorescence signal.[36] These latter two parameters are fundamental to several important relationships across the sciences including the environmental sciences, corrosion and medicine. Cancer cells too are notable for having a more oxidizing and acidic environment than normal non-cancerous cells.[37]

The premise for the design strategy was based on the principles of photoinduced electron transfer (PET) systems.[38] The simplest model (pH sensor) is modular consisting of three components, a fluorophore, a spacer and a receptor, connected in a *fluorophore–spacer–receptor* format (Fig. 4).[39] Excitation of the fluorophore with light begins several possible excited state deactivation pathways; the two of significance for sensing applications are PET and fluorescence. In the 'off' state, electron transfer from the receptor to the excited state fluorophore shuts off the fluorescence. In the 'on' state, fluorescence is observed due to the binding of an analyte to the receptor, which causes emission of light. The most common fluorescent pH sensor consists of an amine connected to an organic fluorophore by a short alkyl spacer.

Another modular model (pE sensor) is the *fluorophore–spacer–electron-donor* format responsive to oxidants.[40] The target is an oxidant (or reductant) rather than an analyte. Electron transfer from an electron-rich redox donor quenches the excited state of the fluorophore. Oxidation of the electron donor causes the electron donor to become electron deficient resulting in a singly occupied molecular orbital to a radical cation. Ferrocene is a well-behaved one-electron donor. Upon oxidation of ferrocene by removal of an electron, the energetics for PET are much less favourable as the absence of charge repulsion due to the singly occupied orbital lowers the ferrocene energy level resulting in fluorescence.

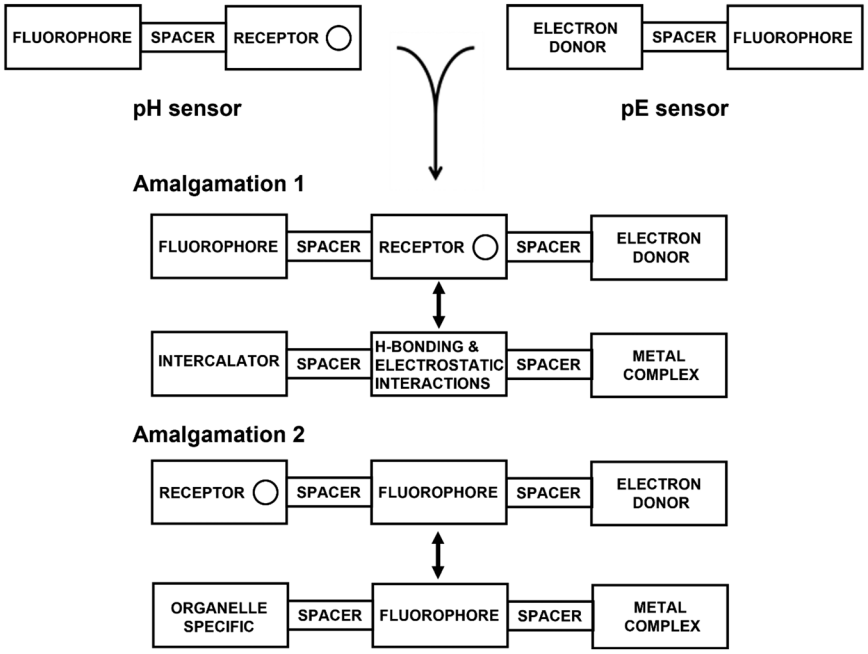

Fig. 4 Comparison of the similarities in the molecular design of fluorescent molecular logic gates, cellular fluorescent imaging probes and organometallic drug entities.

Fluorescent sensors for both pH and pE have practicality in cell biology.[41,42] Fluorescent indicators (pH sensors) for measuring intracellular pH in the cytosol and organelles of live cells have long been commercially available, such as LysoSensor Green (a naphthalimide indicator) and LysoSensor Blue.[43,44] These fluorescent probes have weak nitrogen bases that selectively concentrate in acidic organelles such as lysosomes upon protonation. Cytotoxicity probes (pE sensors), such as RedoxSensor Red CC-1 and tetrazolium salts, are responsive to the redox potential in cell compartments, but tend to be non-selective.[44] At the time of development, fluorescent probes for monitoring the pH and pE simultaneously in living cell imaging were not available. This invention is now documented in patent databases.[45]

The fusion of these two complementary designs, the *fluorophore–spacer–receptor* and *fluorophore–spacer–electron-donor* formats, created dual-responsive molecules for acidic (pH) and oxidising (pE) conditions, termed Pourbaix sensors.[41] Two predominant designs are used to engineer these intelligent molecules. Amalgamation 1 is the *fluorophore–spacer–receptor–spacer–electron-donor* arrangement, and amalgamation 2 is the *receptor–spacer–fluorophore–spacer–electron-donor* configuration. These two configurations appear regularly in the design of multi-targeting drugs and fluorescent probes.

In amalgamation 1, what may be perceived as a fluorophore to a photochemist is a pharmacophore to a medicinal chemist, which could intercalate with DNA, while what a photochemist perceives as a receptor for protons is a site for hydrogen bonding and electrostatic interactions upon protonation. Furthermore, what may be perceived as an electron donor to a photochemist for shutting down fluorescence is a metal complex to a medicinal chemist, which may bind to a hydrophobic pocket or form a covalent bond with DNA.

Amalgamation 2 is applied routinely by chemical biologists interested in imaging subcellular compartments of cells. A proton receptor with a $pK_a < 5$, such as morpholine, is converted into a targeting ligand for lysosomes. Alternatively, attachment of a positively charged triphenylphosphine group is used for selective mitochondria-targeting (*vide infra*). The fluorophore is embedded centrally where it communicates its location within the cell by emitting a light signal upon irradiation, while the metal complex could be a cytotoxic warhead that could react by reactive oxygen species (ROS) or covalent bond formation.

In the forthcoming sections, organometallic–naphthalimide hybrids are presented as cytotoxic and/or luminescent agents. The reader is encouraged to take notice how often the architectural amalgamation designs 1 and 2, highlighted in Fig. 4, appear, and how the forthcoming molecules fit the four matrix classifications of Fig. 3.

Ferrocene-based drugs

The success with ferrocene-based drugs has come from the modification of essential medicines.[46] Chloroquine **4** is a traditional anti-malarial and tamoxifen **5** is a breast cancer drug (Fig. 5). The mechanism of action of **4** involves interference with the digestion of haemoglobin during the malaria parasite life cycle, but in cancer cells chloroquine

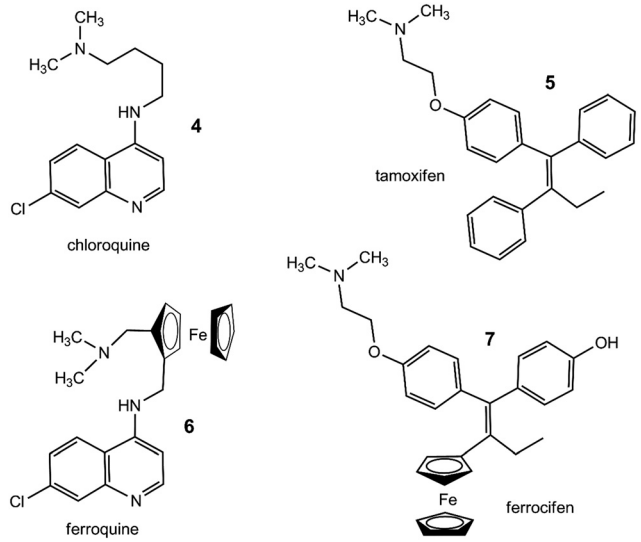

Fig. 5 Chloroquine and tamoxifen are shown as the templates for the ferrocene-based cancer drugs ferroquine and ferrocifen.

produces DNA double strand breaks dependent on ROS.[47] Tamoxifen binds to estrogen receptors producing a complex that decreases DNA synthesis and inhibits estrogen effects.[48] Ferroquine **6** with the clever addition of ferrocene within the linker chain performs the same duty as chloroquine, but with additional mechanisms of action such as the promotion of hydroxyl radical formation that contributes to DNA and cell membrane damage.[49] Like chloroquine, **6** not only accumulates within and deacidifies lysosomes, but it also induces lysosomal membrane permeabilization, mitochondrial depolarization and caspase-independent cancer cell death.[50] The intramolecular H-bonding of the lateral side chain with the heteroaromatic NH within ferroquine improves cross membrane transport and increases the accumulation in the digestive vacuole of the malarial parasite.[51,52] Ferrocifen **7**, a ferrocene–phenol hybrid, has a different mode of action than the anti-cancer Pt drugs, which target DNA directly.[53] In addition to the binding properties to the estrogen receptors as with **5**, ferrocifens are activated by oxidation to reactive quinone methides.[54] It has good efficacy for hormone-dependent (MCF-7, IC_{50} = 0.8 μM) and hormone-independent (MDA-MB-231, IC_{50} = 0.5 μM) breast cancer cells.[55] Analogues with the two-electron donors ruthenocene and osmocene are less cytotoxic.[53]

The elegance of **4** and **5**, from the molecular engineering viewpoint, is the similarity of certain chemical features. Both molecules have planar aromatic systems with a heteroatom at the extremity, either a nitrogen atom or an oxygen atom, and an alkyl chain with a terminal tertiary amine. The connectivity is reminiscent of the *fluorophore–spacer–receptor* formula of the PET system (Fig. 4). The incorporation of ferrocene in **6** introduces the *fluorophore–spacer–electron-donor* format with a methylene spacer inserted in the middle of the chloroquinoline and ferrocene fragments, suggesting the possibility for photo-initiated chemistry (Table 1).

Ferrocene-1,8-naphthalimides

Magri studied eight ferrocenyl-4-amino-1,8-naphthalimides **9–16** *in vitro* against MCF-7 and K562 cancer cell lines by the MTT (3-(4,5-dimethylthiazol-2-yl)-2,5-diphenyltetrazolium

Table 1 Cytotoxicity and mechanisms of action for clinically tested compounds

Compound	Cancer cell lines	IC_{50}/GI_{50} μM (24 hours)	Mechanisms of action	Ref.
1	SKOV-3	1.28	Covalent binding to N7 of guanidine	67
	A549R	9.49		
	HeLa	32.22		
	A549R	2.98		
	HeLa/DDP	12.19		
	HeLa	2.8		
	Endometrial adenocarcinoma	0.034–0.31		
2	Endometrial adenocarcinoma	0.10–0.46	Covalent binding to N7 of guanidine	9
3	SKOV-3	2.77	Covalent binding to N7 of guanidine	67
	A549R	11.73		
	HeLa	17.61		
	A549R	10.42		
4	HCT116	2.27	DNA double strand breaks that depended on ROS	47
5	MCF-7	17.26	Binds to estrogen receptors	48
	BT-474	16.65		
6	HTB-129	8.7	Lysosomal membrane permeabilization, mitochondrial depolarization, inhibition of Akt kinase	50
	Caco-2	101		
7	MDA-MB-231	0.64	Quinine methide reactive species	52
	MCF-7	0.8		
8	EC109	>100	DNA intercalation	59
	BGC-823	80		
	SGC-7901	52		
	Hep G2	35		

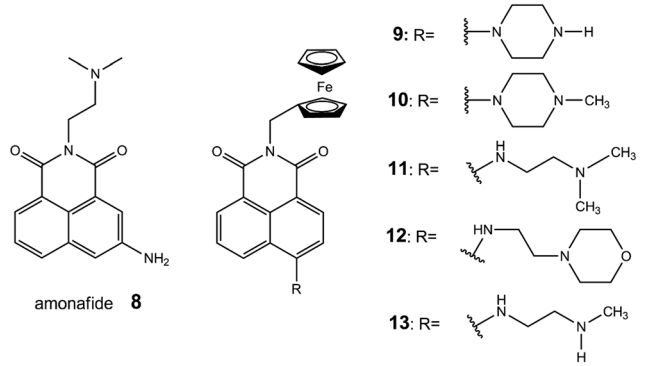

Fig. 6 Comparative model, amonafide **8** and ferrocene–4-amino-1,8-naphthalimides **9**–**13**.

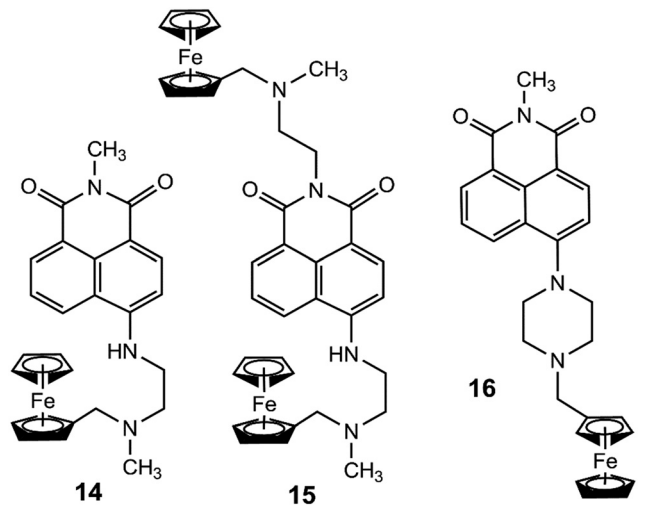

Fig. 7 Ferrocene–naphthalimide compounds **14**–**16**.

bromide) colorimetric assay method.[56] The chemical entities were initially reported as fluorescent logic gates for acidity and oxidisability such as **9**–**12** (Fig. 6).[57–61] Two new entries added a linear methylethylenediamine version **13** and a bis-ferrocene analogue **15**, which was inactive and non-fluorescent. Repurposed as an antiproliferative and cellular imaging agent, **9** with a basic secondary amine ($pK_a > 9.5$) was particularly effective with MCF-7 cells after 24 hours with GI_{50} = 13 μM on par with amonafide **8**. Compounds **10**–**12** with tertiary amines, such as methylpiperazine, dimethylethylenediamine and morpholine, had $GI_{50} > 50$ μM. A model 4-amino-1,8-naphthalimide of **13** without ferrocene has a GI_{50} of 15 μM (K-562), which is 4 times more toxic than **13**.[62] The flexible model **14** had no GI_{50} inhibition after 24 hours, as did methylpiperazine-containing **10** and **16**, and the bis-ferrocene **15**; (Fig. 7) thus within this time window, they are non-toxic fluorescent cellular imaging probes (Fig. 2, top left quadrant). A vibrant green emission was observed from **14** emanating from the nucleus of MCF-7 cells.[56]

Huang investigated two mono-naphthalimide **17** and **18** and eight tripodal ferrocenyl bis-naphthalimide derivatives including **19** and **20** (Fig. 8).[63,64] A hypochromic (downward) effect and red shift were observed in the absorption spectra of **19** and **20** signalling ππ* stacking of at least one naphthalimide between DNA base pairs, which causes the fluorescence emission to decrease. The cytotoxicity was evaluated in four human cancer cell lines (EC109, BGC823, SGC7901 and HEPG2). Derivative **17** is less cytotoxic than the control amonafide in part due to its low solubility in the cell culture medium ($IC_{50} > 100$). The additional ethylene amine linker of **18** aided hydrophilicity and cytotoxicity (IC_{50} = 69–124 μM). The bis-naphthalimides had the hydrocarbon linkers systematically altered from two to six carbons atoms. The cytotoxicity of the bis-naphthalimides is superior across the series (IC_{50} = 0.40–10.18 μM) compared to amonafide **8** (IC_{50} = 35–129 μM) and they are 6–18 times more cytotoxic than the bis-naphthalimide primary amine devoid of the methyleneferrocene.[64] Compounds **19** and **20** are cell

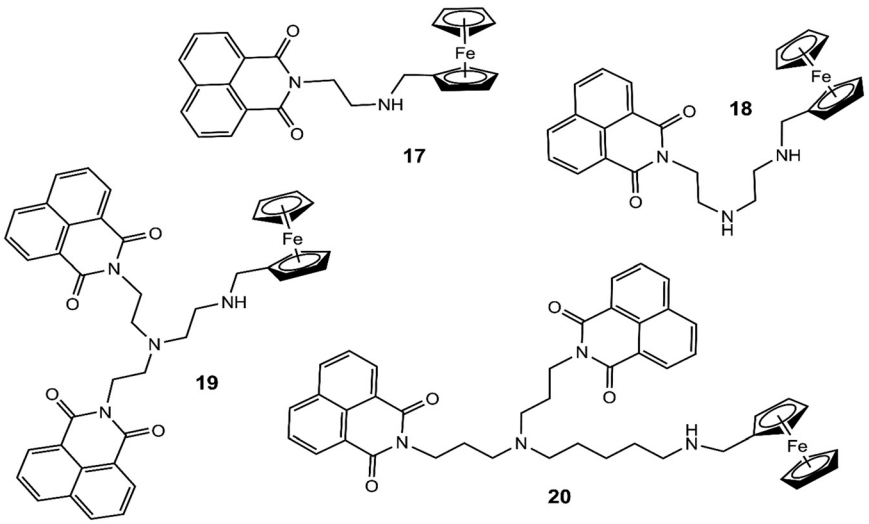

Fig. 8 Mono-naphthalimides **17** and **18** and bis-naphthalimides **19** and **20** with secondary amine and ferrocene moieties.

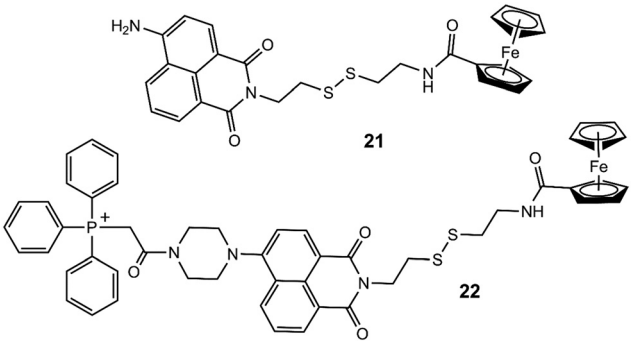

Fig. 9 4-Amino-1,8-naphthalimides **21** and **22** with a ferrocene amide and a disulfide bond. Glutathione cleaves the disulfide bond, which is communicated by a bright fluorescence as the two components diffuse apart. The triphenylphosphine unit is a mitochondrion-directing ligand.

permeable and emit green light predominantly in the cytosol, and to some extent, in the nucleus too. The ferrocene moiety is inferred to generate reactive oxygen species (ROS) by redox chemistry. Incubation of HepG2 cells with **20** resulted in the elevation of cellular ROS levels in a dose-dependent manner 14 times higher than the control.[64] The key finding is that the bis-naphthalimides are more cytotoxic than the mono-naphthalimides. Another study examines bis-naphthyl ferrocenes as DNA-based electrochemical biosensors.[65]

Cao reported two fluorescent probes **21** and **22** with ferrocene and a naphthalimide connected by a disulfide bond linker (Fig. 9).[66,67] Glutathione (GSH) is abundant in healthy cells (1–10 mM) and even more abundant in cancer cells (10–40 mM). A positively charged triphenylphosphine for selective mitochondria-targeting appears in **22**. Both complexes are weakly emissive due to PET from the ferrocene to the excited state 4-amino-1,8-naphthalimide. The fluorescence quantum yield (Φ_F) of **21** is 0.036, while a model without ferrocene (Naph–SS–Boc) has a Φ_F of 0.245. In the presence of GSH, dissociative cleavage of the disulfide bond results in the release of the fluorescent Naph–SH species, which emits vibrant green fluorescence. The probes are insensitive to pH at about physiological levels and have good selectivity and sensitivity to GSH, although they are also responsive to cysteine and homocysteine. The cytotoxicity of **21** and **22** is moderate at 25 μM with the cell survival rate at 75% after 24 hours.[66] *In vivo* testing included two normal cells (HUVEC or LO2) and three cancer cells (SMMC, CT-26 and HepG2). The incubation time for the imaging studies was limited to 2 hours. The fluorescence radiating from the cancer cells is 2–3 times more than that from the HUVEC cells suggesting that the probes can be used for distinguishing normal cells from cancer cells. A hemicyanine analogue has also been demonstrated (Table 2).[68]

Table 2 IC_{50} values of ferrocene-1,8-naphthalimides and summary of mechanisms of action

Compound	Cancer cell lines	IC_{50}/GI_{50} μM (24 hours)	Mechanisms of action	Ref.
9	K562	75	Unknown	56
	MCF-7	13		
10, **14**, **16**	K562	>100	No effect	56
	MCF-7	>100		
11	K562	65	Unknown	56
	MCF-7	52		
12	K562	60	Unknown	56
	MCF-7	>100		
13	K562	62	Unknown	56
	MCF-7	>100		
15	K562	98	Unknown	56
	MCF-7	90		
17	EC109	>100	Poor solubility – no effect	63
	BGC-823	>100		
	SGC-7901	>100		
	Hep G2	>100		
18	EC109	>100	Partial DNA intercalation	63
	BGC-823	88		
	SGC-7901	69		
	Hep G2	>100		
19	EC109	10.52	DNA intercalation & ROS generation	63
	BGC-823	7.76		
	SGC-7901	4.33		
	Hep G2	6.79		
20	EC109	5.28	DNA intercalation & ROS generation	64
	BGC-823	3.40		
	SGC-7901	4.96		
	Hep G2	3.24		
21	Hep G2	>100	Reacts with glutathione	66
22	SMMC	>100	Reacts with glutathione	67

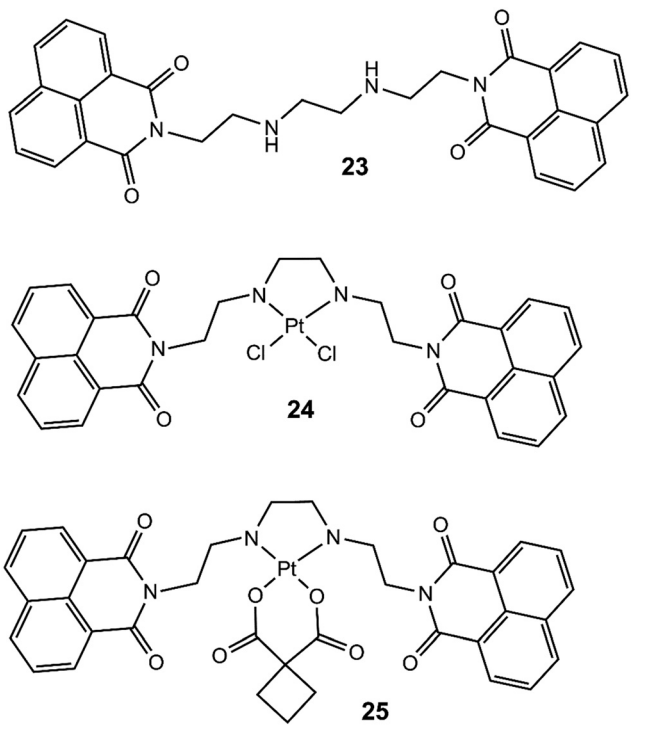

Fig. 10 A strategy for using a polyamine bis-naphthalimide **23** as a carrier molecule for platinum anticancer agents **24** and **25**.

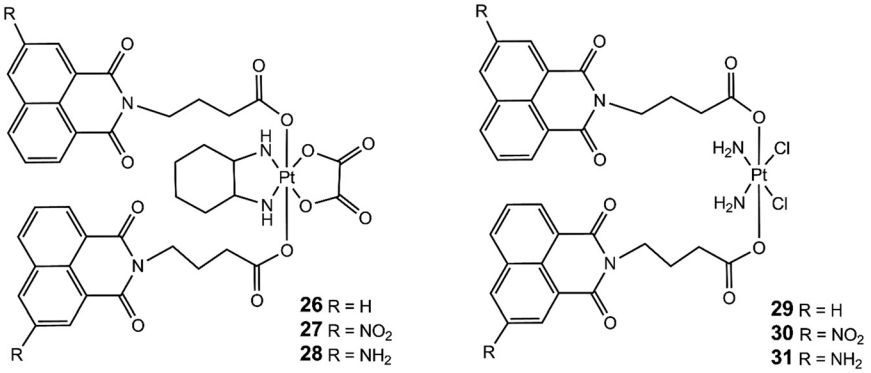

Fig. 11 Bis-naphthalimides linked to Pt(IV) oxaliplatin **26**–**28** and cisplatin **29**–**31** analogues.

Platinum-1,8-naphthalimides

A bis-naphthalimide **23** with an ethylene linker between secondary amines was selected as a transporter for Pt complexes.[69] In hindsight, it seems logical for the bis-naphthalimide DNA intercalator to be combined with cisplatin and carboplatin motifs as with **24** and **25** (Fig. 10).[70,71] *cis*-$Pt(NH_3)_2$ binding to cellular DNA is believed to occur at two neighbouring guanine bases at the N7 atoms. These bis-naphthalimides function as transport molecules for the *cis*-$Pt(NH)_2Cl_2$ and cyclo *cis*-$Pt(CO_2)C(CH_2)_3$ to the DNA in the nucleus. Interaction with plasmid DNA causes conformational changes that are surmised to result from a synergistic effect of intercalation and platination. The better resistance factors of **24** and **25** in relation to cisplatin against all cell lines suggest that the DNA adducts formed by both compounds are different from those of cisplatin. The cytotoxicity of **24** and **25** was 0.28 μM and 0.25 μM in human ovarian tumour cell line A2780, and 1.00 μM and 0.80 μM for cisplatin resistant cells. By comparison, the IC_{50} values for **23** are 10 μM and 100 μM, respectively. The cellular imaging and the effect of Pt on the naphthalimide emission was not reported in 1999. The key takeaway is that a bis-naphthalimide diamino ligand can be used as a "carrier" molecule for infiltrating a *cis*-Pt(II) agent to a DNA target.

Wang and Li demonstrated Pt(IV) carriers **26**–**31** as prodrugs for the Pt(II) drugs oxaliplatin[72] and cisplatin[73] by covalently linking to create bis-naphthalimides (Fig. 11). A dual DNA damage mechanism occurs by targeting and intercalating with DNA *via* the naphthalimide fragment followed by degradation to Pt(II) compounds and naphthalimide carboxylic acid. The release of Pt(II) species induces secondary DNA lesions. The naphthalimide core was further modified with 3-nitro moieties **27** and **30** or 3-amino moieties **28** and **31** as historically used with amonafide and mitonafide, but provided no added benefit. The antitumor activities against five cell lines ovarian cancer (SKOV-3), lung cancer (A549) and cervical cancer (HeLa) and two cisplatin resistant cells A549R and HeLa/DDP had moderately effective antitumor efficacy. An aliphatic three-carbon chain linkage between the naphthalimides and ester (IC_{50} = 3.12–21.37 μM) was optimal compared to one- and two-carbon chains (IC_{50} = 21.81–38.27 μM and 7.71–30.25 μM). UV-vis absorption and fluorescence spectroscopy confirmed intercalation with ct-DNA in a tetravalent form. The circular dichroism spectrum is characterized by a negative peak at 245 nm and a positive peak at 275 nm attributed to the right-handed helicity and base stacking of dsDNA.

Mono-naphthalimide Pt(IV) complexes **32**–**36** have greater aqueous solubility than the above mentioned bis-naphthalimides (Fig. 12).[74,75] Synergetic DNA damage to cancer cells is proposed from the naphthalimide and Pt fragments. Single digit IC_{50} values are reported for SKOV-3 (2.8–3.6 μM) and HeLa (2.8–3.6 μM) cancer cell lines,[75] which are comparable to cisplatin. The IC_{50} values for A549 and A549R were higher at 7.3–17.2 μM. Selectivity for CT26 was observed for **33** (IC_{50} = 3.2 μM). With the longer propionyl chain, **36** once again had the greatest cytotoxicity. In the full study,[75] the linker was varied from 2–4 carbon atoms. There is a wide spectrum of antitumor activities with IC_{50} values < 26.5 μM for all cancer cell lines. The IC_{50} values for SKOV-3 (2.8–3.6 μM) and HeLa (2.8–3.6 μM) cancer cell lines are comparable to that of cisplatin, while those of A549 and A549R were higher at 7.3–17.2 μM. The best candidate **34** was tested in mice bearing CT26 xenograft tumours and found to effectively inhibit tumour growth. A UV-vis absorption displacement experiment indicates intercalations with ct-DNA *via* the naphthalimide fragment evidenced by an absorption peak at 340 nm and the fluorescence at 505 nm is observed to decrease.

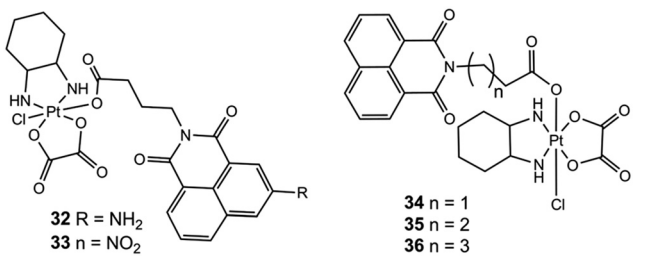

Fig. 12 Naphthalimide platinum(IV) derivatives **32**–**36** containing oxaliplatin with dual DNA damaging mechanisms.

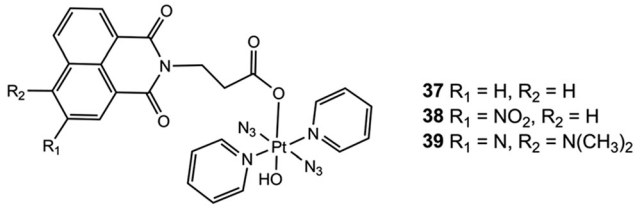

Fig. 13 Photoactive diazido Pt(IV)–naphthalimides **37**–**39** undergo photodecomposition upon irradiation with visible light of 420 nm or 463 nm.

Three photoactive diazido Pt(IV)–naphthalimide complexes **37**–**39** by the Sadler group are dark-stable, even in the presence of GSH (Fig. 13).[76] These complexes undergo decomposition with release of the azide moieties upon irradiation with visible light (420 nm or 463 nm). Emission is observed from **37** and **39** upon irradiation communicating the release of the axial naphthalimide ligand. The 4-nitro-1,8-naphthalimide agent **38** is non-fluorescent. The compounds pre-intercalate with DNA bases through electrostatic interactions by π stacking of the naphthalimide ligand. Linear dichroism indicates that **37** and **38** interact with double-stranded ct-DNA, oriented parallel to DNA base pairs. They form crosslinks by binding to guanine bases. By contrast, **39** did not provide any induced dichroism bands suggesting that it does not bind to DNA, or that its binding affinity is weak, probably due to the bulky 4-NMe_2 ligand. The 4-NMe_2 substituent induces red-shifted absorbance to 450 nm allowing for photodecomposition with 517 nm green light, which gives rise to its photo-cytotoxicity. Induced photo-oxidation of NADH gave rise to ROS suggesting a secondary mechanism. Testing *in vivo* was performed with A2780 ovarian, A549 lung, and PC3 prostate cancer cells, and MRC5 lung normal cells. Dark stability was observed for **36** and **37** with IC_{50} values >50 μM and >100 μM, respectively, while upon irradiation, the IC_{50} values ranged from 1.2–13.5 μM. A review on photoactive and luminescent transition metal complexes as photodynamic therapy agents provides a good reading material for those interested.[77]

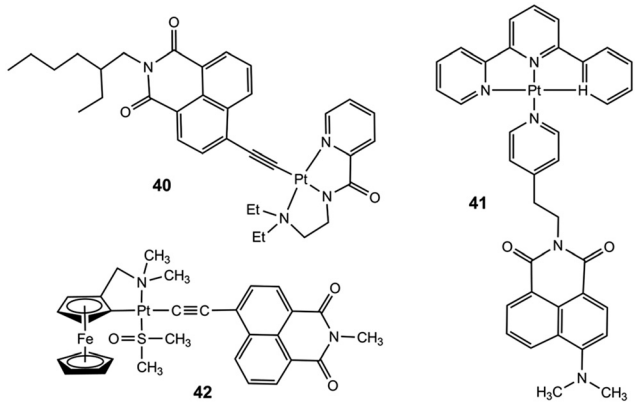

Fig. 14 Alternative ways of combining naphthalimides with Pt **40** and **41** and with Pt-Fe **42** metal complexes.

Wang examined a Pt-based naphthalimide **40** as a PDT agent (Fig. 14).[78] Non-reactive to DNA in the dark, upon irradiation with 425 nm light, ROS are produced killing the cancer cells. Confocal imaging with the fluorescent probe DCFH-DA suggests that $O_2^{\bullet-}$ and $^{\bullet}OH$ are generated. The fluorescence at 623 nm is sensitive to the O_2 concentration. The singlet oxygen quantum yield is 0.86%, which is higher than that of hematoporphyrin PS (0.65%). The electron-withdrawing nitrogen group improves the capture of visible light. No significant change was observed in the ellipticity of both the positive (~275 nm) and negative (~245 nm) ct-DNA bands suggesting that there is no binding to DNA. Instead, the mechanism of action is mitochondrial membrane potential disruption, which induces cell apoptosis. Cellular uptake in MCF-7 cancer cells occurred mainly in the nucleus and mitochondria. The dark cytotoxicity was moderate at 12 M (normoxia) and 24 M (hypoxia). Photoactivation with 825 nm light improved the cytotoxicity to 0.85 μM from 4.01 μM. A weakness is the lack of specificity for tumour cells.

Gunnlaugsson investigated a Pt(II)-based bifunctional DNA binder **41** with terpyridyl and 4-*N*,*N*-dimethyl amino-1,8-naphthalimide.[79] The absorption spectrum has bands at 340 nm and 324 nm assigned to the π–π* transitions of the terpyridyl ligand and the intense band at 450 nm is the ICT transition of the 4-amino-1,8-naphthalimide. The broad emission band at 550 nm is essentially non-fluorescent in water due to hydrogen bonding and the peri-effect (Φ_f = 0.006) from the encumbered dimethylamino moiety. Replacement of one of the two methyl groups with a hydrogen atom would enhance the fluorescence considerably. The cytotoxicity effect against MCF-7 cells was IC_{50} = 18 μM, three times lower than the 1,8-naphthalimide control without Pt (IC_{50} = 50 μM).

A cycloplatinated ferrocenylamine moiety by Robinson is an untested organometallic–naphthalimide hybrid with two metal centres.[80] Consideration of Pt complexes in combination with ferrocene–naphthalimide analogues such as **42** offers novel prospects for the next generation of chemotherapy candidates. An X-ray crystal structure of an anthraquinone derivative revealed the coordination of dimethylsulfoxide *via* the sulfur atom to Pt. The compound is soluble in chlorinated solvents, acetone and alcohols. The naphthalimide emission is completely quenched in the ground state. However, the emission is partially restored in the ferrocenium oxidised state. The emission at 592 nm is minimally affected by the cycloplatinated ethynyl group. For an inspiring read, see a review by Reedijk, which provides insights into the drug design of novel Pt compounds with another metal centre (Table 3).[81]

Ruthenium-1,8-naphthalimides

Ruthenium compounds have three biologically accessible oxidation states (II, III, and eventually IV) that may overcome the issue of resistance that hinders platinum-based therapeutics.[82] The recent development of TLD1433 (Fig. 15),

43, by McFarland has provided fresh impetus within the organometallic medicinal chemistry community.[83] It is the first ruthenium polypyridyl complex to enter human clinical trials for the PDT treatment of non-invasive muscular bladder cancer. The complex is luminescent and photocytotoxic. Tested in HL-60 human promyelocytic leukemia cells, it is

Table 3 IC_{50} values of platinum-1,8-naphthalimides and summary of mechanisms of action

Compound	Cancer cell lines	IC_{50}/GI_{50} μM (24 hours)	Mechanisms of action	Ref.
23	A2780	>10	DNA intercalation adducts are repaired in CH1cisR cells	71
	A2780cisR	>100		
	CH1	>10		
	CH1cisR	>100		
	Pam212	140		
	Pam212-ras	160		
24 and **25**	A2780	0.28,0.25	DNA intercalation & platination	71
	A2780cisR	1.00, 0.80		
	CH1	0.35, 0.27		
	CH1cisR	0.60, 0.45		
	Pam212	158, 5.20		
	Pam212-ras	89, 10.40		
26–28	SKOV-3	3.12–6.69	Structural change and DNA damage leading to apoptosis	72
	A549R	21.37–77.00		
	HeLa	13.14–33.48		
	A549R	11.79–48.36		
	HeLa/DDP	9.88–31.67		
29	SKOV-3	9.98	Structural change and DNA damage leading to apoptosis	73
	A549	44.47		
	A549R	30.02		
	HeLa	8.64		
	HeLa/DDP	13.09		
30	SKOV-3	2.49	Structural change and DNA damage leading to apoptosis	73
	A549	18.17		
	A549R	20.45		
	HeLa	35.35		
	HeLa/DDP	21.17		
31	SKOV-3	1.28	Structural change and DNA damage leading to apoptosis	73
	A549	3.90		
	A549R	6.53		
	HeLa	5.26		
	HeLa/DDP	3.98		
32	SKOV-3	1.58	DNA intercalation & platination	74
	HeLa	0.96		
	A549	1.65		
	A549R	0.46		
33	SKOV-3	6.4	DNA intercalation & platination	75
	HeLa	2.9		
	A549	9.51		
	A549R	26.5		
	CT26	2.8		
	293 T	9.8		
34–36	SKOV-3	2.8–3.6	DNA intercalation & platination	75
	A549	10.7–17.2		
	A549R	7.3–15.9		
	HeLa	2.0–2.9		
	CT26	3.2–11.1		
	293 T	5.1–14.0		
37	NA	NA	NA	76
38		Dark >50	DNA intercalation & photo-induced cellular ROS	76
	A549	11.8		
	PC3	6.4		
39		Dark >100		
	A2780	13.5		
	A549	10.1		
	PC3	1.2		
40	MCF-7	11.72/0.85	Disrupts the mitochondrial membrane potential and induces cell apoptosis	78
	A549	17.83/2.18		
	A549/CDDP	9.43/1.25		
41	MCF-7	18	Induces apoptosis	79
42	NA	NA	NA	80

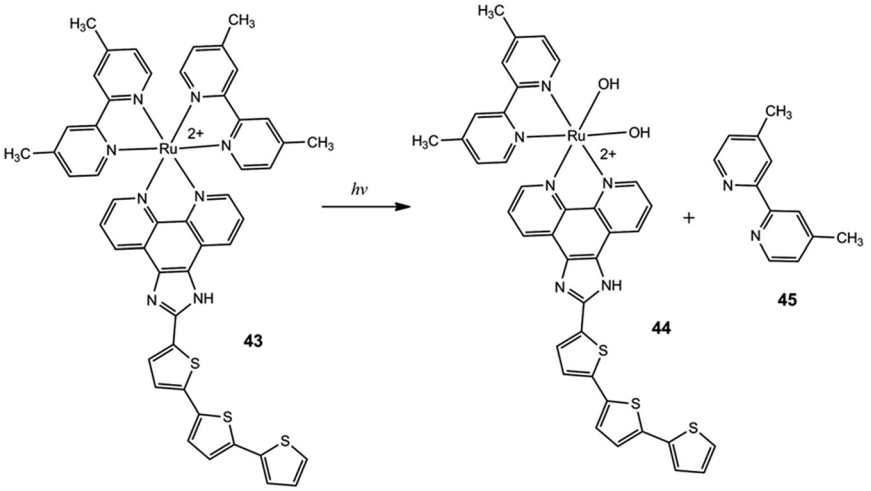

Fig. 15 The ruthenium complex **43**, otherwise known as TLD1433, is currently in clinical trials.

non-toxic in the absence of a light trigger ($IC_{50} > 100$ μM).[84] Upon visible light activation, one of the 6,6′-dimethyl-2,2′-bipyridine ligands **45** is ejected from the complex to yield a dihydro complex **44**. The IC_{50} values are 1.1 μM and 0.2 μM after 1 hour and 16 hours of irradiation, with the latter being fourteen times more cytotoxic than cisplatin (IC_{50} = 2.8 μM). A dual mechanism is proposed consisting of alkylation of DNA and strand breakage by singlet oxygen. The three thiophene units are crucial to elevating the singlet oxygen yield to 42%.

N-heterocyclic carbene (NHC) fragments of 4-ethylthio-1,8-naphthalimides with ruthenium are combined with naphthalimides **46–48** by Ott (Fig. 16). The naphthalimide[85,86] without the metal emits a green emission at 503 nm. Metal incorporation reduces the emission possibly due to a PET mechanism. The anti-proliferative and biological effects in MCF-7 breast cancer and HT-29 colon adenocarcinoma cells are respectable with **46–48** having lower values in HT-29 ($IC_{50} < 11$ μM). The organic ligands void of the metal had a greater cytotoxicity for MCF-7 (IC_{50} 1.5–4.6 μM). The binding constants of the uncomplexed 4-ethylthio-1,8-naphthalimide ligands have higher affinities for DNA than their metal coordinated counterparts by 10-fold. Lipophilicity-dependent cytotoxicity was observed with the benzyl-substituted **48** exhibiting the highest activity. Circular dichroism of ct-DNA and G-quadruplex c-Kit2 G4 provides evidence for strong binding by intercalation and the fluorescence and UV-vis spectroscopy studies highlight dual-interactive modes. Mass spectrometry suggests coordination of the metal centres with the N7 site of guanine. Studies were extended to bis-naphthalimide structures **49** and **50**.[87] The cytotoxic effects are ligand dependent with only a minor influence from the Ru center. The IC_{50} values for MCF-7 and HT-29 cells are 26 μM and > 100 μM for **49**, and 1.7 μM and 3.7 μM for **50**, emphasising the importance of the thioethyl group.

The half-sandwich 1,8-naphthalimide appended Ru(II) complexes **51** and **52** by Patra are useful as real-time cellular imaging agents (Fig. 17).[88] The cumene moiety facilitates cellular uptake due to its lipophilicity and the morpholine is organelle specific for targeting lysosomes. The 1,3,5-triaza-7-phosphatricyclo-[3.3.1.1]decane (PTA) ligand within **52** reduces the hydrolysis rate. Mass spectra [Ru(L)(5′-GMP)] revealed adducts at an *m*/*z* of 966.25 corresponding to $[M–Cl]^+$, indicating Ru(II)/5′-GMP adduct formation at the N7 of 5′-GMP suggesting DNA crosslinking after hydrolysis of the Ru–Cl bonds. From circular dichroism, the ellipticity increases slightly in the positive band, while a large decrease is observed in the negative band suggesting an intercalative mode of action with DNA. Thus, covalent adduct formation *via* hydrolysis of Ru–Cl bonds and intercalative interactions supports two modes of action.

Patra showed the internalization of **51** and **52** *via* endocytosis in MCF-7, A498 and HeLa cells viewed by confocal fluorescence microscopy. Bright green spots are observed inside the nucleus, specifically at the nucleoli (Fig. 18). 4′,6-Diamidino-2-phenylindole (DAPI) was used as a nuclear stain and LysoTracker™ Blue (a morpholino-based PET pH indicator) confirmed localisation in the lysosomes. The interaction with calf thymus DNA was investigated using circular dichroism with both positive and negative changes indicative of intercalative binding.

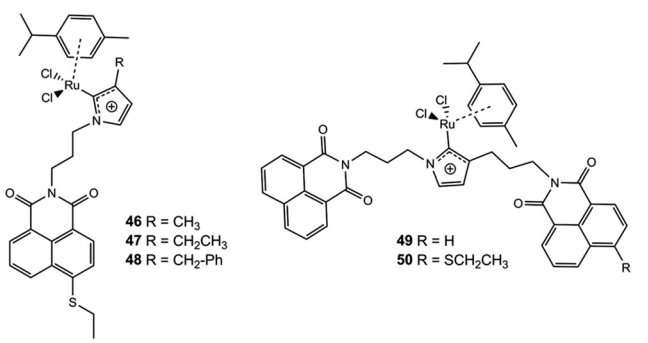

Fig. 16 Ruthenium ethylthio-mono and bis-1,8-naphthalimides **46–50**.

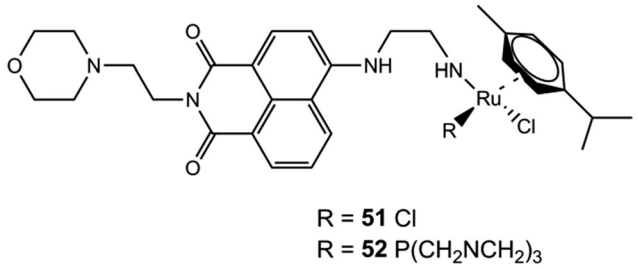

Fig. 17 Half-sandwich Ru(II)-1,8-naphthalimide complexes **51** and **52** as photocytotoxic and fluorescent cellular imaging agents.

Higher cytotoxicity was observed when irradiated with 448 nm LED light *versus* lower toxicity under dark conditions. These Ru(II)–arene complexes could be PDT agents due to their preferential accumulation in the nucleus, where singlet oxygen could react with the cancer cells. The complexes showed light-enhanced toxicity in MCF-7, A498 and HeLa cells, which are 2–3 times more cytotoxic upon light irradiation with IC_{50} of 11.5–20.4 μM for **51** and 15.3–30.0 μM for **52**. The complexes target both the nucleolus and lysosomes suggesting the potential for a synergistic cell-death mechanism.

Sadler reported that the Ru complexes **53–55** have an emission comparable to the free naphthalimide ligands (Fig. 19).[89] Photoactivation was monitored by ^{1}H NMR providing evidence for naphthalimide released upon irradiation and a solvated ruthenium complex coordinated to DMSO. The photodegradation kinetics varied significantly among the complexes. Of the three complexes, **55** demonstrated the fastest photolysis completely decomposing after 3 hours, while **53** and **54** showed less than 50% decomposition within the same period. The cytotoxicity was evaluated with A549 human lung cancer cells using an MTT assay in the dark for 24 hours (IC_{50} = 76.7 μM) followed by 3 hours of light irradiation with 420 nm blue LED light. The

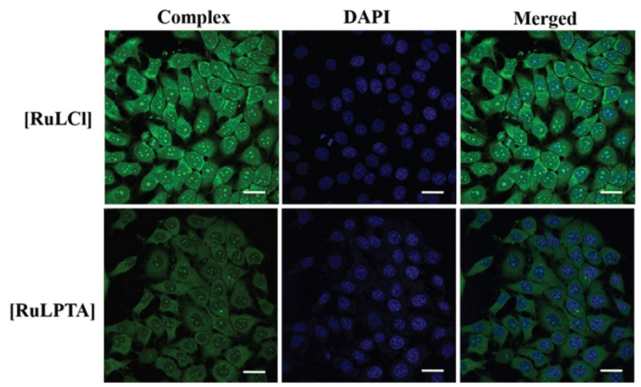

Fig. 18 Confocal laser scanning microscopy (CLSM) images of MCF-7 cells incubated with 10 μM **51** and **52** for 5 h at 37 °C. A blue channel was used for observing DAPI (nuclear staining dye) and a green channel. The merged images highlight nuclear and cytosolic localization. Scale bar: 20 μm. λ_{ex} = 488 nm for Ru complexes, λ_{ex} = 358 nm for DAPI. Reproduced from ref. 88 with permission from the RSC, copyright 2021.

naphthalimide ligands without Ru exhibited no cytotoxicity. The naphthalimide role is to enhance cellular uptake and act as a light-harvesting antenna. Only **55** exhibited any significant photocytotoxicity with an IC_{50} of 10.5 μM correlating with its absorption in the blue region and rapid release of the pyridal-naphthalimide photoproduct.

Gunnlaugsson examined Ru complexes **56** and **57** with flexible pentane linkers connected to naphthalimide (Fig. 20).[90] The bis-naphthalimide **57** is non-toxic upon light irradiation, making it suitable as a fluorescence imaging agent, while the mono-naphthalimide **56** is a chemotherapy candidate. Intramolecular stacking in the ground state causes a 22% reduction in metal–ligand charge transfer (MLCT) absorbance at 459 nm. Single-band emissions are observed at 645 nm and 670 nm with efficient singlet–singlet energy transfer from the naphthalimide to the Ru(II) MLCT state. DNA intercalation is slightly stronger with **57** (1.5×10^7 M^{-1}). The mono-naphthalimide complex enhances metal-centered emission upon DNA binding, whereas the bis-naphthalimide exhibits a more complicated emission profile due to intramolecular stacking with the DNA. Dichroism studies confirm these differing binding modes. Photocleavage assays indicate that **56** efficiently cleaves DNA upon irradiation, while the bis-naphthalimide structure restricts access to molecular oxygen, reducing its photocleavage ability. Confocal microscopy confirms cellular internalization, predominantly in the nucleus. In HeLa cells, **56** has a photocytotoxicity of 7.8 μM.

The spectroscopic properties of rigid Ru-1,4,5,8-tetraazaphenanthrenes (TAP) **58** and **59** and $Ru(bpy)_2$ **60–63** by Gunnlaugsson were studied in phosphate-buffered water (Fig. 21).[91,92] MLCT-based emissions at 645 nm and 625 nm are due to efficient energy transfer from the naphthalimide to the Ru(II)-based MLCT state. Electron transfer between the Ru(II) center and the naphthalimide moiety quenches the MLCT excited state. The amino substituent of **59** exhibited more efficient quenching than the nitro-substituted **58**, while the reverse trend was observed for the $Ru(bpy)_2$ complexes. The 1,8-naphthalimide is proposed to bind by intercalation and the Ru(II) center by external binding to DNA. Binding constants are of the order of 10^6–10^7 M^{-1}. UV-vis and circular dichroism spectroscopy studies are suggestive of tight association with the DNA grooves. MTT assays of **60–63** in

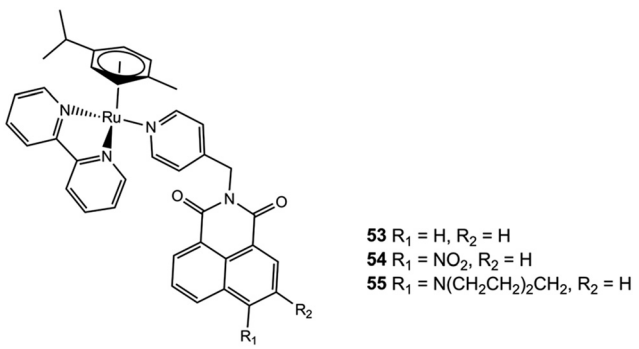

Fig. 19 Photoactivitable ruthenium–naphthalimide complexes **53–55**.

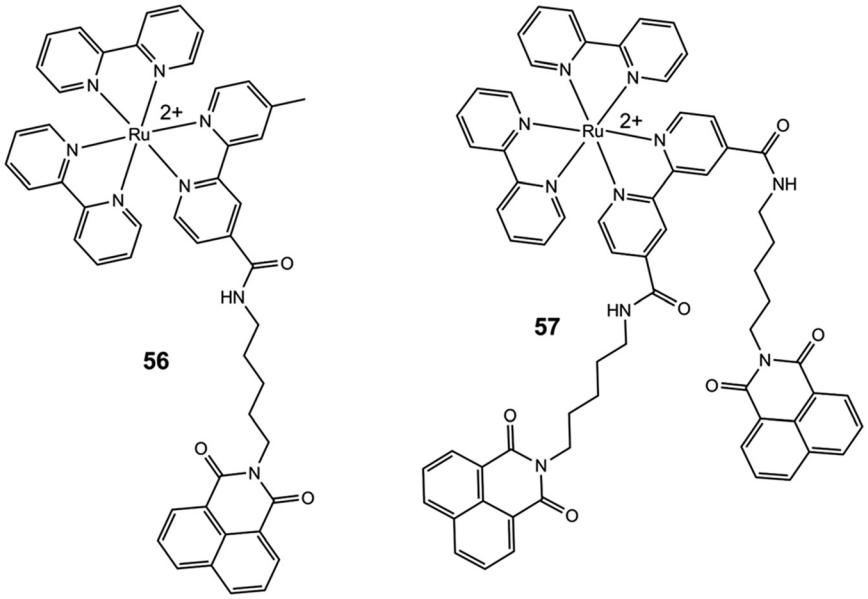

Fig. 20 Ruthenium(II) polypyridyl complexes **56** and **57** with 1,8-naphthalimide groups as DNA binders.

K562 cells indicated that the 4-nitro derivative **60** exhibited dark cytotoxicity, while 4-amino derivatives **61** and **63** showed no dark toxicity. The phototoxicity of **61** was 24.4 μM. Light dose-dependent increases in phototoxicity correlated with DNA photocleavage activity. Flow cytometry with dihydroethidium provided evidence for ROS generation upon photoactivation. Studies on related compounds to **62** and **63** are efficient dual topoisomerases I and IIα poisons.[93]

Gunnlaugsson converted 4-amino-1,8-naphthalimides into bis-naphthalimide Tröger bases.[94] In a latest study, the mechanism of cellular uptake and trafficking was probed by **64** and **65** (Fig. 22).[95] They are readily taken up by HeLa cancer cells within hours by caveolae and lipid raft-dependent endocytosis. Localisation was observed primarily in the lysosomal and Golgi apparatus, with some accumulation in mitochondria, but conspicuously, no entry was observed into the nucleus. Activation with light increased ROS production and altered tubulin eventually resulting in apoptotic cell death. Without light, the compounds are non-toxic at 10 μM concentrations, while the phototoxicity is significant at 1.8 μM and 4.6 μM. Imaging by confocal microscopy relied on an argon laser with excitation at 488 nm to generate emission at 620 nm.

Tröger bases are amalgamated with two *p*-cumene Ru(II) complexes to yield **66** (Fig. 23).[96] Fluorescence in CH_2Cl_2 is

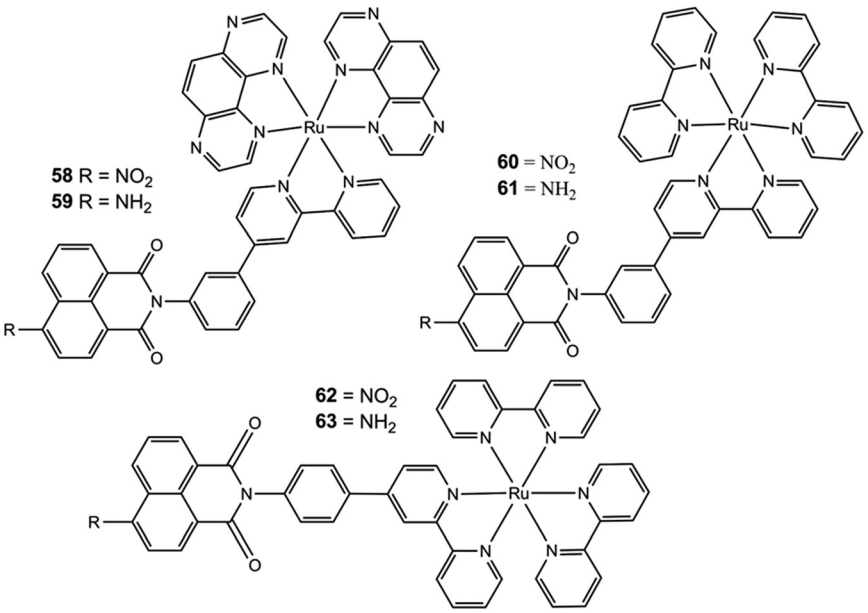

Fig. 21 Ruthenium(II) 1,8-naphthalimide complexes **58**–**63** with TAP or bpy ligands.

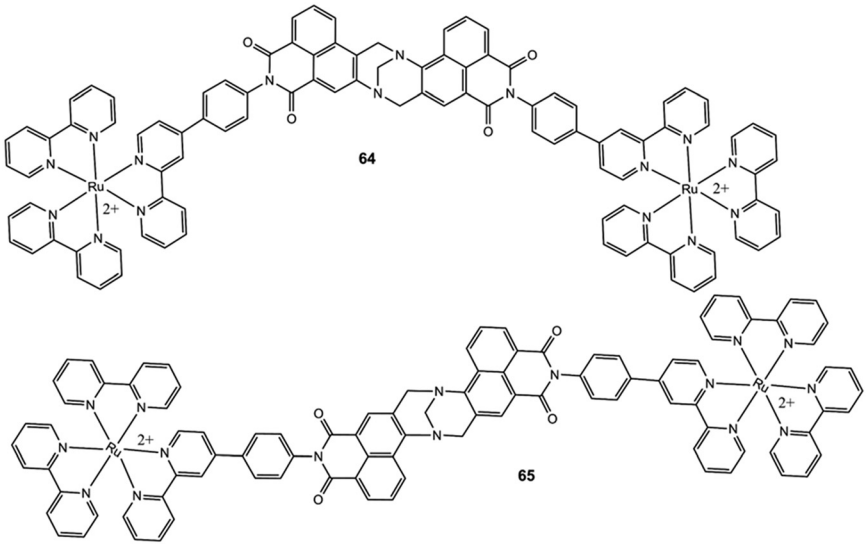

Fig. 22 Supramolecular complexes **64** and **65** incorporating ruthenium(II) 1,8-naphthalimide structures with Tröger base linkages.

centred at 511 nm (Φ_F = 0.135), while unmetalled model **67** showed a red-shifted emission at 511 nm (Φ_F = 0.242). The *p*-cumene Ru(II) complex **68** is non-fluorescent. Energy transfer is corroborated by spectral overlap of the bis-naphthalimide emission and curcumin absorption explaining the lower Φ_F of **67**. Molecular orbital calculations identify the HOMO localized on the Ru(II) centres and the LUMO residing on the 1,8-naphthalimides. The cellular uptake of **66** within HeLa, HCT-116, and HepG2 cancer cells occurs within minutes localizing in the cytoplasm and near the edge of the nucleus, although no fluorescence was detected in HCT-116 and HepG2 cells likely due to poor cellular uptake or weak emissivity. Membrane blebbing in HepG2 cells was observed possibly due to apoptosis or necrosis. The hybrid **66** is cytotoxic after 48 hours in all three cell lines (IC_{50} = 2.0 μM in HeLa cells) in contrast to **67**, which is not cytotoxic (IC_{50} > 100 μM) while the Ru–curcumin fragment **68** is moderately cytotoxic (IC_{50} = 16 μM). Analogues of **67** with propyl and ethylenedimethylamine moieties have IC_{50} values of 75 μM and 2.4 μM.[97] A Ru(II) complex features the isoquinoline alkaloid, papaverine, as a phototoxicity agent against Hs578T breast cancer and A375 melanoma cells (Table 4).[98]

Iridium, rhenium and rhodium 1,8-naphthalimides

Iridium complexes are another promising alternative to traditional Pt-based chemotherapies that can interact with

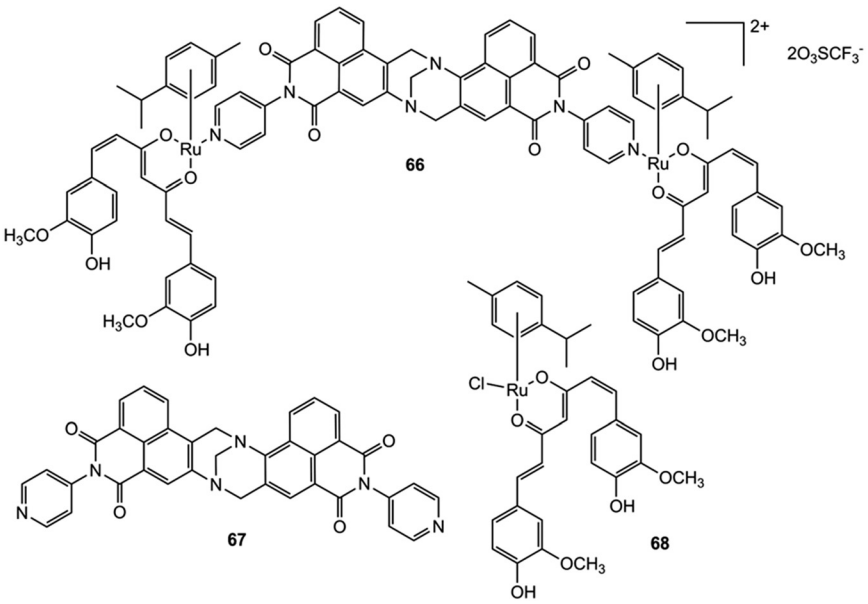

Fig. 23 A 4-Amino-1,8-naphthalimide Tröger base **66** bridged to Ru(II)–curcumin scaffolds.

Table 4 IC_{50} values of ruthenium-1,8-naphthalimides and summary of mechanisms of action

Compound	Cancer cell lines	IC_{50}/GI_{50} μM (24 hours)	Mechanisms of action	Ref.
43	HeLa	150 (dark)	Ru bond formation	84
44	HeLa	0.2 (light)	Ru bond formation	84
45	NA	NA	Photo labile ligand	84
46	MCF-7	18.6		85
	HT-29	36.8		
47	MCF-7	11.6		85
	HT-29	26.4		
48	MCF-7	4.8		85
	HT-29	4.9		
49	MCF-7	26.0		86
	HT-29	>100		
50	MCF-7	1.7	DNA intercalation	86
	HT-29	3.7		
51	MCF-7	16.7	Toxic in the dark and	88
	A498	20.4	with 448 nm light	
	HeLa	11.5	compared to healthy cells with HeLa	
52	MCF-7	30.0	Toxic in the dark and	88
	A498	16.6	with 448 nm light	
	HeLa	15.3	compared to healthy cells with HeLa	
53 and **54**	A549	>100 (dark) >100 (light)	NA	89
55	A549	76.7 (dark) 10.5 (light)	Unknown	89
56	HeLa	29.8 (dark) 7.81 (light)	DNA intercalation Light-induced DNA cleavage	90
57	HeLa	>30 (dark) >30 (light)	DNA interaction	90
58	K562	20.9 71.2 (dark) 69.6	DNA interaction & groove binding	92
59	K562	22.4 >100, 24.4	DNA photocleavage	92
60	K562	21.2 >100, 73		92
61	K562	32.0 >100, 53.4	DNA photocleavage	92
62	HeLa	>10 (dark) 1.8 (light)	ROS in mitochondria DNA damage	94
63	HeLa	>10 (dark) 4.6 (light)	ROS in mitochondria DNA damage	94
64	HeLa	2.0		96
	HCT-116	2.7		
	Hep G2	1.9		
65	HeLa	>100	NA	96
	HCT-116	>100		
	Hep G2	>100		
66	HeLa	15		96
	HCT-116	16		
	Hep G2	17		

multiple biomolecules, including proteins, enabling them to bypass common resistance mechanisms.[99] The half-sandwich iridium complexes **69–71** by Liu were tested with A549, HeLa and HepG2 cancer cells and Beas-2b normal cells (Fig. 24). The methyl derivative **69** was inactive (IC_{50} > 100 μM). The incorporation of the biphenyl group on the cyclopentadiene ring significantly improved the anticancer activity of **70** and **71** (IC_{50} = 4.9–17.1 μM). Better anticancer activity was

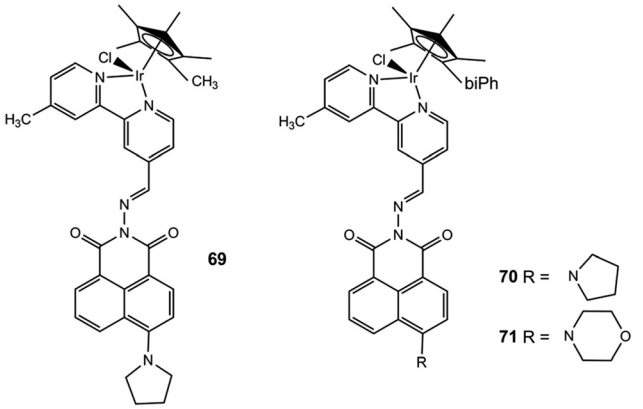

Fig. 24 Iridium half-sandwich complexes.

observed with A549 and HepG2 compared to cisplatin (IC_{50} = 7.5–22.7 μM).[100] Changing the central metal ion to Ru resulted in loss of anti-proliferative ability. Binding occurs with BSA complex 2, which interferes with the S phase and G2/M phase of the cells, decreases the mitochondrial membrane potential and significantly increases intracellular reactive oxygen species (ROS). Complex **70** successfully targets mitochondria after energy-dependent entry into the mitochondria and causes apoptosis by inducing mitochondrial autophagy, while complex **71** targets lysosomes.[101]

Rhenium complexes are an underestimated class of organometallic anticancer agents.[102] Re(I) complexes **72–75** are biocompatible offering bright emission at 530 nm in methanol and tuneable photophysical properties by confocal fluorescence microscopy (Fig. 25).[103] Structural tuning of the *N*-alkyl substituents allowed for fine control of the cellular uptake and localization. The microscopy revealed varied uptake and localization of the ligands. The free naphthalimide ligand exhibited negligible cellular uptake due to limited permeability. While **72** had good uptake and even distribution within the cytoplasm, **73** had good uptake and mitochondrial localization. With **74**, bright fluorescence and precise mitochondrial labelling was observed, even in apoptosis-related processes, such as plasma membrane

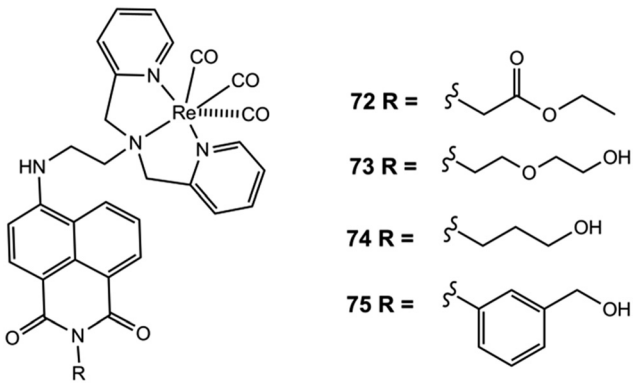

Fig. 25 A series of rhenium(I) picolyl-containing compounds **72–75** wiht various moieties at the imide end.

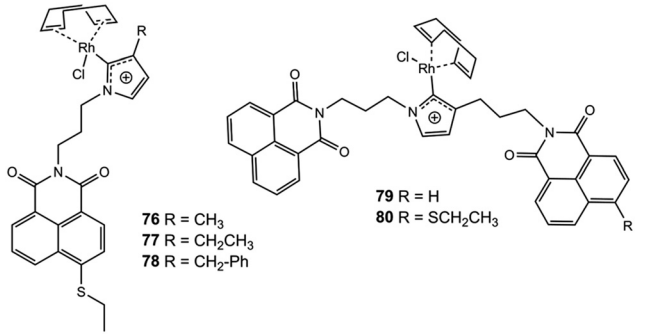

Fig. 26 Rhodium N-heterocyclic carbene naphthalimide complexes **76**–**80**.

Table 5 IC_{50} values of iridium, rhenium and rhodium 1,8-naphthalimides and summary of mechanisms of action

Compound	Cancer cell lines	IC_{50}/GI_{50} μM (24 hours)	Mechanisms of action	Ref.
69	A549	>100	NA	100
	HeLa	>100		
	Hep G2	>100		
	Beas-2B	>100		
70	A549	15.6	Mitochondria	100
	HeLa	11.3	Cell arrest in the S phase	
	Hep G2	11.8	and G2/M phase	
	Beas-2B	14.0	Increase in ROS levels	
71	A549	17.0	Permeabilizing the	100
	HeLa	17.1	lysosomal	
	Hep G2	4.9	Membrane	
	Beas-2B	16.4		
72–75	NA		No IC study performed	103
76	MCF-7	5.8	DNA intercalation	86
	HT-29	10.0		
77	MCF-7	1.7	DNA intercalation	86
	HT-29	6.5		
78	MCF-7	4.0	DNA intercalation	86
	HT-29	6.2		
79	MCF-7	14.7		87
	HT-29	>100		
80	MCF-7	2.6	DNA covalent bond to Rh	87
	HT-29	2.7		

blebbing and cytoplasmic vacuolation, while **75** showed no uptake. The 3-propanol derivative **74** emerged as the most favourable candidate, balancing cellular uptake efficiency with mitochondrial localization.

Rhodium(I) N-heterocyclic carbenes **76**–**78** were evaluated for their antiproliferative effects, cellular uptake and DNA-binding activity (Fig. 26).[86] The cytotoxicity for all three compounds is good (IC_{50} 1.7–10.0 μM). Cytotoxicity increases with increasing alkyl functional group lipophilicity (methyl < ethyl < benzyl) at position 3 of the imidazole ring. The uptake into tumour cells was studied in MCF-7 cells with **76** and **77**. Replacement of the metal centre with Rh *versus* Ru increased the cytotoxic activity 3–4-fold while the activity for **78** was like the Ru analogue. The 4-ethylthio group on the naphthalimide results in a strong blue fluorescence emission. Fluorescence quenching is more pronounced for these Rh derivatives than with the Ru analogues discussed above suggesting a more efficient PET. An intense emission was detected after 30 min upon treatment with 10 mM in MCF-7 cells. The solubility in water was better with **77** than with **76**, which was excluded from some analysis. A weak induced CD band is observed for **78** at 400 nm suggesting intercalation as the binding mode. Studies with nucleobase 9-ethylguanine by mass spectrometry demonstrated that upon loss of the chloride ligand, a covalent bond forms at the Rh centre. The bis-naphthalimides **79** and **80** were both cytotoxic to MCF-7 cells with IC_{50}s of 14.7 μM and 2.6 μM.[87] In contrast, with HT29 cells **79** was completely inactive while **80** retained a cytotoxicity of 2.7 μM (Table 5).

Conclusions and perspectives

This review highlights recent advancements with dual-purpose metal-based agents, with primarily Fe, Pt and Ru with cytotoxicity and/or luminescence properties based on 1,8-naphthalimides. A classification system for categorising cytotoxic and/or luminescent compounds (Fig. 3) and a molecular engineering template based on the amalgamation of modular components connected by a spacer or linker were proposed (Fig. 4). While notable progress has been made, such as with metal N-heterocyclic carbenes,[104] the field remains in its early stages, with few dual-purpose drug candidates reaching even preclinical application. Theranostic metal–naphthalimide complexes hold great promise for gaining insights from the cellular level to preclinical *in vivo* studies.

1,8-Naphthalimide compounds are generally good DNA intercalators and emissive compounds. However,

Table 6 List of cell lines and their respective cell type

Cell line	Cell type	Cell line	Cell type
A2780	Ovarian cancer	HeLa	Cervical cancer
A375	Skin melanoma	Hep G2	Hepatocellular carcinoma
A498	Kidney cancer	HT-29	Colon cancer
A549	Lung cancer	HTB-129	Breast ductal carcinoma
Beas-2B	Non-cancerous bronchial epithelium	K562	Erythroleukemia
BGC-823	Gastric cancer	MDA-MB-231	Breast cancer
BT-474	Breast carcinoma	MCF-7	Breast cancer
CH1	Gastric cancer – attributed to the CDH1 gene	Pam212	Mouse squamous skin carcinoma
Caco-2	Colorectal adenocarcinoma	PC3	Prostate cancer
EC109	Esophageal squamous cell carcinoma	SGC-7901	Gastric cancer
HCT116	Colorectal carcinoma	SKOV-3	Ovarian cancer

1,8-naphthalimides with nitro, primary amines and dimethylamino continue to be frequently studied, even though they often provide no additional cytotoxic synergy. Furthermore, historical evidence with amonafide (3-NH_2) and mitonafide (3-NO_2) prohibited them as viable therapeutic agents due to excessive toxicity (bone marrow) from acetylated metabolites resulting from oxidation of the amine and nitro moieties. Secondary amines tend to show better cytotoxicity than primary amines likely due to better solubility and enhanced electrostatic interactions. Nitro and dimethylamino substituents directly attached to the aromatic scaffold are detrimental to the luminescence. N-heterocycles (piperazine, morpholine, pyrrolidine), monoalkylamino (NH), alkoxyalkyl (OR) and thioalkyl (SR) provide highly fluorescent compounds, but are mostly limited to green emission. Extension of the absorbance and emission to the near infra-red (NIR) by conjugation of the naphthalimide with another fluorophore allows for photodynamic therapy applications.[105]

Organometallic compounds offer a range of metal oxidation states, coordination numbers and geometries, such as *cis* and *trans*. They offer different redox centres that may promote reactive oxygen species. The addition of ferrocene to tamoxifen introduced an alternative mechanism of action by redox chemistry on oxidative metabolism to generate quinone methides. Conjugation of ferrocene with the naphthalimide scaffold, rather than separation by an alkyl spacer, could bring about new reactivity. The excellent DNA binding and targeting ability of naphthalimides allows them to be carriers of Pt and Ru complexes that can covalently bond to DNA. There are many more metal complexes to be explored.

New drugs are sought for two major reasons: to reduce toxicity and to circumvent cell resistance. By photoirradiation, ligands can be removed selectively with control. Selectivity can be achieved by activating the drug while at the target site. The use of light to trigger a photocytotoxic state as with TLD1433 reduces side effects as activity only occurs where the light source is applied.[84] Selectivity could also come from one or more chemical triggers found only in cancer cells or found at higher concentrations than in non-cancerous cells, such as glutathione,[66,67] or higher acidity and oxidisability,[56] which could then activate the drug and communicate the event by a luminescence signal.

Abbreviations

A list of cell lines and their respective cell type is provided in Table 6.

Data availability

There are no additional data available.

Conflicts of interest

There are no conflicts of interest to declare.

Acknowledgements

The University of Malta and the Ministry of Education, Sport, Youth, Research and Innovation are gratefully acknowledged for a Reach High II post-doctoral scholarship awarded to ADJ.

References

1 NIH National Cancer Institute, **https://www.cancer.gov/about-cancer/understanding/what-is-cancer**.
2 World Health Organization, Cancer, **https://www.who.int/news-room/fact-sheets/detail/cancer**.
3 M. A. Fuertes, C. Alonso and J. M. Pérez, *Chem. Rev.*, 2003, **103**, 645–662.
4 D. Wang and S. J. Lippard, *Nat. Rev. Drug Discov.*, 2005, **4**, 307–320.
5 E. Proschak, H. Stark and D. Merk, *J. Med. Chem.*, 2019, **62**, 420–444.
6 R.-G. Fu, Y. Sun, W.-B. Sheng and D.-F. Liao, *Eur. J. Med. Chem.*, 2017, **136**, 195–211.
7 B. Meunier, *Acc. Chem. Res.*, 2008, **41**, 69–77.
8 B. Rosenberg, L. VanCamp, J. E. Trosko and V. H. Mansour, *Nature*, 1969, **222**, 385–386.
9 (*a*) R. Canetta, M. Rozencweig and S. K. Carter, *Cancer Treat. Rev.*, 1985, **12**, 125–136; (*b*) V. Rantanen, S. Grenman, J. Kulmala and R. Grenman, *Br. J. Cancer*, 1994, **69**, 482–486.
10 J.-L. Misset, *Br. J. Cancer*, 1998, **77**, 4–7.
11 P. Chellan and P. J. Sadler, *Chem. – Eur. J.*, 2020, **26**, 8676–8688.
12 S. Banerjee, E. B. Veale, C. M. Phelan, S. A. Murphy, G. M. Tocci, L. J. Gillespie, D. O. Frimansson, J. M. Kelly and T. Gunnlaugsson, *Chem. Soc. Rev.*, 2013, **42**, 1601–1618.
13 A. Kamal, N. R. Bolla, P. S. Srikanth and A. K. Srivastava, *Expert Opin. Ther. Pat.*, 2013, **23**, 299–317.
14 R. Tandon, V. Luxami, H. Kaur, N. Tandon and K. Paul, *Chem. Rec.*, 2017, **17**, 956–993.
15 M. D. Tomczyk and K. Z. Walczak, *Eur. J. Med. Chem.*, 2018, **159**, 393–422.
16 R. Tandon, V. Luxami, N. Tandon and K. Paul, *Bioorg. Chem.*, 2022, **121**, 105677.
17 W. Ruan, Z. Xie, Y. Wang, L. Xia, Y. Guo and D. Qiao, *Molecules*, 2024, **29**, 4529.
18 S. Ganesan and A. Sheela, *Chem. Pap.*, 2024, **78**, 8531–8561.
19 J. L. Nitiss, *Nat. Rev. Cancer*, 2009, **9**, 338–350.
20 Z. Chen, X. Liang, H. Zhang, H. Xie, J. Liu, Y. Xu, W. Zhu, Y. Wang, X. Wang, S. Tan, D. Kuang and X. Qian, *J. Med. Chem.*, 2010, **53**, 2589–2600.
21 L. Wang, M. Fujii, M. Yamaji and H. Okamoto, *Photochem. Photobiol. Sci.*, 2018, **17**, 1319–1328.
22 A. D. Johnson, K. Szaciłowski and D. C. Magri, *Dyes Pigm.*, 2024, **231**, 112424.
23 E. E. Rudebeck, R. P. Cox, T. D. M. Bell, R. Acharya, Z. Feng, N. Gueven, T. D. Ashton and F. M. Pfeffer, *Chem. Commun.*, 2020, **56**, 6866–6869.

24 J. Kypr, I. Kejnovská, D. Renčiuk and M. Vorlíčková, *Nucleic Acids Res.*, 2009, **37**, 1713–1725.
25 B. Bertrand, P. E. Doulain, C. Goze and E. Bodio, *Dalton Trans.*, 2016, **45**, 13005–13011.
26 B. Henderson, *The Product Portfolio*, Boston Consulting Group (BCG), 1970.
27 S. Venugopal, V. Sharma, A. Mehra, I. Singh and G. Singh, *Chem. Biol. Drug Des.*, 2022, **100**, 580–598.
28 A. S. Biebricher, I. Heller, R. F. H. Roijmans, T. P. Hoekstra, E. J. G. Peterman and G. J. L. Wuite, *Nat. Commun.*, 2015, **6**, 7304.
29 H.-K. Liu and P. J. Sadler, *Acc. Chem. Res.*, 2011, **44**, 349–359.
30 S. S. Kelkar and T. M. Reineke, *Bioconjugate Chem.*, 2011, **23**, 1879–1903.
31 B. E. Bowler, K. J. Ahmed, W. I. Sundquist, L. S. Hollis, E. E. Whang and S. J. Lippard, *J. Am. Chem. Soc.*, 1989, **111**, 1299–1306.
32 W. I. Sundquist, D. P. Bancroft and S. J. Lippard, *J. Am. Chem. Soc.*, 1990, **112**, 1590–1596.
33 E. Bodio, P. Le Gendre, F. Denat and C. Goze, Development of Trackable Anticancer Agents Based on Metal Complexes, in *Advances in Inorganic Chemistry*, Elsevier, 2016, ch. 6, vol. 68, pp. 253–299.
34 T. C. Pham, V.-N. Nguyen, Y. Choi, S. Lee and J. Yoon, *Chem. Rev.*, 2021, **121**, 13454–13619.
35 D. C. Magri, G. J. Brown, G. D. McClean and A. P. de Silva, *J. Am. Chem. Soc.*, 2006, **126**, 4950–4951.
36 D. C. Magri, *Front. Chem.*, 2024, **12**, 1393308.
37 X. Huang, *Mutat. Res.*, 2003, **533**, 153–171.
38 A. J. Bryan, A. P. de Silva, S. A. de Silva, R. A. D. D. Rupasinghe and K. R. A. S. Sandanayake, *Biosensors*, 1989, **4**, 169–179.
39 A. P. de Silva, T. S. Moody and G. D. Wright, *Analyst*, 2009, **134**, 2385–2393.
40 D. C. Magri, *Analyst*, 2015, **40**, 7487–7495; D. C. Magri, *Analyst*, 2017, **142**, 676.
41 D. C. Magri, *Supramol. Chem.*, 2017, **29**, 741–748.
42 T. J. Farrugia and D. C. Magri, *New J. Chem.*, 2013, **37**, 148–151.
43 A. P. de Silva and R. A. D. D. Rupasinghe, *J. Chem. Soc., Chem. Commun.*, 1985, 1669–1670.
44 I. Johnson and M. T. Z. Spence, *The Molecular Probes Handbook: A Guide to Fluorescent Probes and Labelling Technologies*, Life Technologies Corporation, U.S., 11th edn, 2010.
45 (*a*) D. C. Magri and J. C. Spiteri, Sensor molecule, a method of measuring acidity and redox potential, *UK IPO Pat.*, GB2533166B, 2020; (*b*) D. C. Magri and J. C. Spiteri, *US Pat. Application*, US2016169850A1, 2015.
46 World Health Organization List of Essential Medicines, 23rd list, WHO, 2023, **https://www.who.int/publications/i/item/WHO-MHP-HPS-EML-2023.02**.
47 D. Iglesias-Corral, P. García-Valles, N. Arroyo-Garrapucho, E. Bueno-Martínez, J. Manuel Ruiz-Robles, M. Ovejero-Sánchez, R. González-Sarmiento and A. Belén Herrero, *Front. Oncol.*, 2024, **14**, 1390518.
48 M. Suicmez, G. Namalir and H. Ozdil, *Journal of the Institute of Science and Technology*, 2023, **13**, 2997–3006.
49 D. Dive and C. Biot, *ChemMedChem*, 2008, **3**, 383–391.
50 A. Kondratskyi, K. Kondratska, F. Vanden Abeele, D. Gordienko, C. Dubois, R.-A. Toillon, C. Slomianny, S. Lemière, P. Delcourt, E. Dewailly, R. Skryma, C. Biot and N. Prevarskaya, *Sci. Rep.*, 2017, **7**, 15896.
51 F. Dubar, C. Slomianny, J. Khalife, D. Dive, H. Kalamou, Y. Guérardel, P. Grellier and C. Biot, *Angew. Chem., Int. Ed.*, 2013, **125**, 7844–7847.
52 G. Jaouen, A. Vessières and S. Topa, *Chem. Soc. Rev.*, 2015, **44**, 8802–8817.
53 Y. Wang, P. Pigeon, S. Top, M. J. McGlinchey and G. Jaouen, *Angew. Chem., Int. Ed.*, 2015, **54**, 10230–10233.
54 S. Top, J. Tang, A. Vessières, D. Carrez, C. Provot and G. Jaouen, *Chem. Commun.*, 1996, 955–956.
55 H. Z. S. Lee, O. Buriez, F. Chau, E. Labb, R. Ganguly, C. Amatore, G. Jaouen, A. Vessières, W. K. Leong and S. Top, *Eur. J. Inorg. Chem.*, 2015, 4217–4226.
56 A. D. Johnson, J. A. Buhagiar and D. C. Magri, *RSC Med. Chem.*, 2021, **12**, 2060–2064.
57 M. Vella Refalo, N. V. Farrugia, A. D. Johnson, S. Klejna, K. Szaciłowski and D. C. Magri, *J. Mater. Chem. C*, 2019, **7**, 15225–15232.
58 J. C. Spiteri, A. D. Johnson, S. A. Denisov, G. Jonusauskas, N. D. McClenaghan and D. C. Magri, *Dyes Pigm.*, 2018, **157**, 278–283.
59 J. C. Spiteri, S. A. Denisov, G. Jonusauskas, S. Klejna, K. Szaciłowski, N. D. McClenaghan and D. C. Magri, *Org. Biomol. Chem.*, 2018, **16**, 6195–6201.
60 A. D. Johnson, K. A. Paterson, J. C. Spiteri, S. A. Denisov, G. Jonusauskas, A. Tron, N. D. McClenaghan and D. C. Magri, *New J. Chem.*, 2016, **40**, 9917–9922.
61 J. C. Spiteri, J. S. Schembri and D. C. Magri, *New J. Chem.*, 2015, **39**, 3349–3352.
62 A. D. Johnson, R. Zammit, J. Vella, M. Valentino, A. J. Buhagiar and D. C. Magri, *Bioorg. Chem.*, 2019, **93**, 103287.
63 D. G. Jia, J. A. Zheng, Y. R. Fan, J. Q. Yu, X. L. Wu, B. J. Wang, X. B. Yang and Y. Huang, *J. Organomet. Chem.*, 2019, **888**, 16–23.
64 Y.-R. Fan, B. J. Wang, D.-G. Jia, X.-B. Yang and Y. Huang, *J. Inorg. Biochem.*, 2021, **219**, 111425.
65 Y.-R. Deng, Y.-F. Li, H. Tang, Y.-R. Fan and Y. Huang, *J. Inorg. Biochem.*, 2024, **257**, 112615.
66 G. J. S. Cheng, J. M. Qin, X. Li and Q. Y. Cao, *Dyes Pigm.*, 2023, **211**, 111089.
67 X. Li, H. Wang, Y. Zhang, Q. Y. Cao and Y. Chen, *Chin. Chem. Lett.*, 2021, **32**, 1541–1544.
68 X. Zhao, X. Zeng, X. Wu, L. Shi, S. Zhu and W. Sun, *Chemosensors*, 2023, **11**, 397.
69 M. F. Braña, J. M. Castellano, M. Morán, M. J. Pérez de Vega, C. R. Romerdahl, X. D. Qian, P. Bousquet, F. Emling, E. Schlick and G. Keilhauer, *Anti-Cancer Drug Des.*, 1993, **8**, 257–268.
70 P. F. Bousquet, M. F. Braña, D. Conlon, K. M. Fitzgerald, D. Perron, C. Cocchiaro, R. Miller, M. Moran, J. George, X.-D. Qian, G. Keilhauer and C. A. Romerdahl, *Cancer Res.*, 1995, **55**, 1176–1180.

71 J. M. Pérez, I. López-Solera, E. I. Montero, M. F. Braña, C. Alonso, S. P. Robinson and C. Navarro-Ranninger, *J. Med. Chem.*, 1999, **42**, 5482–5486.
72 Q. P. Wang, X. X. Tan, Z. F. Liu, G. S. Li, R. Y. Zhang, J. J. Wei, S. B. Wang, D. C. Li, B. Q. Wang and J. Han, *Eur. J. Pharm. Sci.*, 2018, **214**, 127–136.
73 Q. P. Wang, G. S. Li, Z. F. Liu, X. X. Tan, Z. Ding, J. Ma, L. J. Li, D. Li, J. Han and B. Q. Wang, *Eur. J. Inorg. Chem.*, 2018, 4442–4451.
74 Q. P. Wang, Y. Chen, G. S. Li, Y. Zhao, Z. F. Liu, R. Y. Zhang, M. Liu, D. C. Lia and J. Han, *Bioorg. Med. Chem. Lett.*, 2019, **29**, 126670.
75 Z. J. Li, Y. Chen, Z. F. Liu, Q. P. Wang, Y. Zhao, J. J. Wei, M. Liu, Z. P. Wang, D. C. Li and J. Han, *Monatsh. Chem.*, 2020, **151**, 353–367.
76 H. Shi, J. Kasparkova, C. Soulié, G. J. Clarkson, C. Imberti, O. Novakova, M. J. Paterson, V. Brabec and P. J. Sadler, *Chem. – Eur. J.*, 2021, **27**, 10711–10716.
77 B. S. McGhie and J. R. Aldrich-Wright, *Biomedicines*, 2022, **10**, 578.
78 Y. Wang, X. Shi, H. Fang, Z. Han, H. Yuan, Z. Zhu, L. Dong, Z. Guo and X. Wang, *J. Med. Chem.*, 2022, **65**, 7786–7798.
79 S. Banerjee, J. A. Kitchen, S. A. Bright, J. E. O'Brien, D. C. Williams, J. M. Kelly and T. Gunnlaugsson, *Chem. Commun.*, 2013, **49**, 8522–8524.
80 E. M. McGale, R. E. Murray, C. J. McAdam, J. L. Morgan, B. H. Robinson and J. Simpson, *Inorg. Chim. Acta*, 2003, **352**, 129–135.
81 J. Reedijk, *Eur. J. Inorg. Chem.*, 2009, 1303–1312.
82 S. Thota, D. A. Rodrigues, D. C. Crans and E. J. Barreiro, *J. Med. Chem.*, 2018, **61**, 5805–5821.
83 S. Monro, K. L. Colón, H. Yin, J. Roque, P. Konda, S. Gujar, R. P. Thummel, L. Lilge, C. G. Cameron and S. A. McFarland, *Chem. Rev.*, 2019, **119**, 797–828.
84 T. Sainuddin, M. Pinto, H. Yin, M. Hetu, J. Colpitts and S. A. McFarland, *J. Inorg. Biochem.*, 2016, **158**, 45–54.
85 W. Streciwilk, A. Terenzi, R. Misgeld, C. Frias, P. G. Jones, A. Prokop, B. K. Keppler and I. Ott, *ChemMedChem*, 2017, **12**, 214–225.
86 W. Streciwilk, A. Terenzi, X. Cheng, L. Hager, Y. Dabiri, P. Prochnow, J. E. Bandow, S. Wölfl, B. K. Keppler and I. Ott, *Eur. J. Med. Chem.*, 2018, **156**, 148–161.
87 W. Streciwilk, A. Terenzi, F. Lo Nardo, P. Prochnow, J. E. Bandow, B. K. Keppler and I. Ott, *Eur. J. Inorg. Chem.*, 2018, 3104–3112.
88 P. Srivastava, M. Verma, A. Kumar, P. Srivastava, R. Mishra, S. Sivakumar and A. K. Patra, *Dalton Trans.*, 2021, **50**, 3629–3640.
89 F. Bisceglie, G. Pelosi, N. Orsoni, M. Pioli, M. Carcelli, P. Pelagatti, S. Pinelli and P. J. Sadler, *Int. J. Mol. Sci.*, 2022, **23**, 7624.
90 G. J. Ryan, F. E. Poynton, R. B. P. Elmes, M. Erby, D. C. Williams, S. J. Quinn and T. Gunnlaugsson, *Dalton Trans.*, 2015, **44**, 16332–16344.
91 G. J. Ryan, S. Quinn and T. Gunnlaugsson, *Inorg. Chem.*, 2008, **47**, 401–403.
92 R. B. P. Elmes, G. J. Ryan, M. L. Erby, D. O. Frimannsson, J. A. Kitchen, M. Lawler, D. C. Williams, S. J. Quinn and T. Gunnlaugsson, *Inorg. Chem.*, 2020, **59**, 10874.
93 S. A. Murphy, C. A. Phelan, E. B. Veale, O. Kotova, S. Comby and T. Gunnlaugsson, *Org. Biomol. Chem.*, 2021, **19**, 6817–6833.
94 Y. Sun, J. Li, H. Zhao and L. Tan, *J. Inorg. Biochem.*, 2016, **163**, 88–94.
95 S. A. Bright, M. L. Erby, F. E. Poynton, D. Monteyne, D. Pérez-Morga, T. Gunnlaugsson, D. C. Williams and R. B. P. Elmes, *RSC Chem. Biol.*, 2024, **5**, 344–359.
96 B. Mohan, S. Estalayo-Adrian, D. Umadevi, B. la Cour Poulsen, S. Blasco, G. J. McManus, T. Gunnlaugsson and S. Shanmugaraju, *Inorg. Chem.*, 2022, **61**, 11592–11599.
97 S. Shanmugaraju, B. la Cour Poulsen, T. Arisa, D. Umadevi, H. L. Dalton, C. S. Hawes, S. Estalayo-Adrián, A. J. Savyasachi, G. W. Watson, D. C. Williams and T. Gunnlaugsson, *Chem. Commun.*, 2018, **54**, 4120–4123.
98 G. Sanità, M. L. Alfieri, B. Carrese, S. Damian, V. Mele, G. Calì, B. Silvestri, S. Marra, S. Mohammadi, G. Luciani, P. Manini and A. Lamberti, *RSC Med. Chem.*, 2024, **16**, 779–790.
99 W. Ma, S. Zhang, Z. Tian, Z. Xu, Y. Zhang, X. Xia, X. Chen and Z. Liu, *Eur. J. Med. Chem.*, 2019, **18**, 111599.
100 P. Szymaszek, M. Tyszka-Czochara and J. Ortyl, *Eur. J. Med. Chem.*, 2024, **276**, 116648.
101 F. Bisceglie, G. Pelosi, N. Orsoni, M. Pioli, M. Carcelli, P. Pelagatti, S. Pinelli and P. J. Sadler, *Int. J. Mol. Sci.*, 2022, **23**, 7624.
102 A. Leonidova and G. Gasser, *ACS Chem. Biol.*, 2014, **9**, 2180–2193.
103 E. E. Langdon-Jones, N. O. Symonds, S. E. Yates, A. J. Hayes, D. Lloyd, R. Williams, S. J. Coles, P. N. Horton and S. J. A. Pope, *Inorg. Chem.*, 2014, **53**, 3788–3797.
104 H. Amouri, *Chem. Rev.*, 2023, **123**, 230–270.
105 D. C. Magri and A. A. Camilleri, *Chem. Commun.*, 2023, **59**, 4459–4462.